MEDICAL ROBOTS

Anti-inflammatory therapy enables robot-actuated regeneration of aged muscle

S. L. McNamara[1,2], B. R. Seo[1,2†], B. R. Freedman[1,2], E. B. Roloson[1,2], J. T. Alvarez[1], C. T. O'Neill[1], H. H. Vandenburgh[3], C. J. Walsh[1,2], D. J. Mooney[1,2*]

Robot-actuated mechanical loading (ML)–based therapies ("mechanotherapies") can promote regeneration after severe skeletal muscle injury, but the effectiveness of such approaches during aging is unknown and may be influenced by age-associated decline in the healing capacity of skeletal muscle. To address this knowledge gap, this work used a noninvasive, load-controlled robotic device to impose highly defined tissue stresses to evaluate the age dependence of ML on muscle repair after injury. The response of injured muscle to robot-actuated cyclic compressive loading was found to be age sensitive, revealing not only a lack of reparative benefit of ML on injured aged muscles but also exacerbation of tissue inflammation. ML alone also disrupted the normal regenerative processes of aged muscle stem cells. However, these negative effects could be reversed by introducing anti-inflammatory therapy alongside ML application, leading to enhanced skeletal muscle regeneration even in aged mice.

INTRODUCTION

Skeletal muscle aging leads to a progressive loss in muscle mass and strength as well as the capacity of muscles to recover from injury, ultimately compromising physical performance and resulting in functional limitations (*1*). Elderly patients experience higher rates of complications (*2*, *3*), longer hospital stays (*4*), and an inability to fully regain function after injury (*5*). This regenerative decline is due to intrinsic impairments in aged muscle stem cell behavior and numerous age-associated changes in the muscle microenvironment, including the immune system, a key component of muscle repair (*6*–*9*). Age-related dysfunctions in the immune response, termed immunosenescence or "inflammaging," lead to a state of chronic inflammation after injury and have been linked to poor regenerative outcomes in the elderly (*10*–*13*). Furthermore, because the treatment of geriatric muscle injuries using operative or pharmacological measures can be limited by medical contraindications in elderly patients, alternative noninvasive therapies that instead rely on the use of physical tissue manipulation, such as massage, may offer a safer alternative (*14*, *15*).

Regenerative robotics is an actively emerging field aimed at developing technologies that can promote tissue healing by leveraging the biophysical sensing capabilities of the body. The development of noninvasive robot-based mechanical loading (ML) therapies (also called "mechanotherapies") has been explored particularly for skeletal muscle repair given its well-known sensitivity to mechanical cues. Muscle stem cells exhibit strong activation and proliferation behavior in response to ML (*16*–*19*), and after injury, mechanotherapy has been shown to offer therapeutic benefit by enhancing muscle function, improving structural repair of damaged myofibers, and reducing tissue fibrosis in a variety of in vivo models (*20*–*24*). Recent work has also demonstrated an immunomodulatory role of ML after muscle injury (*20*, *25*). Specifically, immune down-regulation and the clearance of inflammatory cells, including neutrophils, from the tissue have been linked to positive outcomes of ML-based therapies (*23*, *24*). However, most of the data produced thus far on these therapies and their mechanisms derive from studies done in young animals. Given the numerous physiological changes that occur with age and the ever-growing elderly population, a better understanding of how regenerative robotic therapies exert their biological effects and how these effects change as the body ages is critical to inform clinical studies for different age groups.

In this work, we evaluated the effects of robot-actuated ML on aged muscle after severe injury using a force feedback–controlled robotic compressive loading device. The severe injury model used here is relevant for studying geriatric trauma (*3*, *5*) where satellite-cell driven regenerative capacity remains intact (*26*). On the basis of previous reports of the immunoregulatory role of ML in the regeneration of young muscle (*21*, *24*, *25*), we hypothesized that ML would promote aged muscle repair by down-regulating the chronic aged inflammatory response while simultaneously stimulating the aged stem cell population. We instead observed that the same ML parameters that confer a benefit on young muscle after injury are ineffective at facilitating recovery in injured aged muscle. Moreover, a notable exacerbation of inflammation was found in injured aged muscles in response to ML, as well as a disruption in the regenerative behavior of aged muscle stem cells. We sought to test whether these negative effects of ML on injured aged muscle could be alleviated with inflammatory control. We found that this was the case—robot-actuated ML hindered aged muscle regeneration on its own, but combining ML with glucocorticoid (GC) therapy reversed these negative effects and enabled aged muscle regeneration after severe injury.

[1]John A. Paulson School of Engineering and Applied Sciences, Harvard University, Cambridge, MA, USA. [2]Wyss Institute for Biologically Inspired Engineering, Harvard University, Boston, MA, USA. [3]Department of Pathology and Laboratory Medicine, Brown University, Providence, RI, USA.
*Corresponding author. Email: mooneyd@seas.harvard.edu
†Present address: Takeda Pharmaceuticals, Thousand Oaks, CA, USA.

RESULTS

Aged muscle exhibits impaired healing and an altered immune response after severe injury

This work modeled severe muscle injury using a two-step process consisting of intramuscular myotoxin injection into the tibialis anterior (TA) muscle followed by induction of hindlimb ischemia (Fig. 1A). Myotoxin induces severe necrosis in muscle fibers while leaving the extracellular matrix intact and sparing the satellite cell population (*27*), and femoral artery ligation of the hindlimb exacerbates and prolongs the injury (*21*, *24*, *28*, *29*). We first investigated the differences in recovery of severely injured TA muscles from young (2- to 3-month-old) and aged (20- to 22-month-old) animals. As illustrated in Fig. 1, we observed significantly impaired healing in aged muscles. By 14 days after injury, tetanic contraction forces elicited from injured young muscles matched those of uninjured young muscles, whereas even by day 21, injured aged muscles could not generate tetanic contraction forces greater than 35% of those of uninjured aged muscles (Fig. 1B). Furthermore, significantly lower fatigue resistance was observed in aged muscles compared with young muscles after consecutive stimulations (Fig. 1C), as well as lower TA–to–body weight ratios (Fig. 1D). Structurally, at 14 days after injury, aged muscles exhibited a higher percentage of damaged myofibers and a greater degree of fibrosis than young muscles, with more frequent presence of calcification and adipose deposits as seen on hematoxylin and eosin (H&E)– and Masson's trichrome–stained sections (Fig. 1, E and F). $Pax7^+$ cells in aged and young muscle were quantified to evaluate the proliferative response of muscle stem cells after injury. Although Pax7 is expressed by quiescent muscle stem cells (also called satellite cells), it is also expressed on activated muscle stem cells [also called myogenic precursor cells (MPCs)]. These MPCs make up a majority of the $Pax7^+$ cells observed in the stained muscle sections, and this staining pattern is consistent with what has been observed in other studies evaluating muscle stem cell response to injury (*24*, *30*, *31*). Total $Pax7^+$ cells in uninjured aged and young muscle were similar; however, a greater increase in $Pax7^+$ cells was observed in young muscle at 3 days after injury compared with aged muscle, indicating a more robust proliferative response of the young MPC population (Fig. 1, G and H).

Because the inflammatory response to muscle injury is a critical determinant of regeneration, we performed flow cytometry analysis of immune cell populations in injured aged and young tissue during recovery. Total immune cells ($CD45^+$) in injured young muscles peaked at day 3 and subsequently declined to baseline. In aged muscle, however, a blunted immune response was observed with significantly lower immune cell numbers at day 3 compared with young tissue, as well as a later peak at day 7 (Fig. 1I). Because intramuscular immune cell numbers in young muscle were in steady decline by day 7 and other studies investigating muscle regeneration in young animals have observed similar intramuscular immune cell kinetics (*32*–*34*), the day 10 time point was not analyzed for this age group to avoid unnecessary use of animals. Infiltrating immune cell subtypes were identified as neutrophils ($CD11b^+/CD11c^-/F4/80^-/Ly6g^+/Ly6c^{int}$), macrophages ($CD11b^+/CD11c^-/F4/80^+$), and dendritic cells ($CD11b^+/CD11c^+$). Neutrophils, the earliest responder in the inflammatory cascade, peaked in both young and aged injured muscle by day 3, with significantly higher numbers observed in young muscle at day 1 compared with aged muscle, followed by a rapid return to baseline in both groups (Fig. 1J). Macrophages and dendritic cells, which are key regulators of muscle stem cell behavior, peaked early in young muscle at day 3 (Fig. 1, K and L). In aged muscle, however, the intramuscular peak in these cells occurred between days 7 and 10 and was followed by a delay in inflammatory resolution, as indicated by a slower return of the cell numbers to uninjured baseline values (Fig. 1, K and L, and fig. S1). Together, these findings confirm impaired recovery of aged muscle after severe injury, with less robust MPC and immune cell responses and delayed resolution of inflammation compared with young muscle.

Robot-actuated ML promotes recovery of young but not aged muscle after severe injury

A robotic loading device with a soft elastomeric interface was used to apply cyclic compressive loading to the TA muscle of the injured hindlimb (Fig. 2, A to C). The actuator was equipped with force feedback control to ensure consistent, repeatable loading across treatment sessions and between animals. To prevent deflection or translation of the muscle during actuation, a rigid U-shaped limb holster was used to support the limb, and the ankle was secured with a silicone tie as shown in Fig. 2B. Severely injured young and aged TA muscles were subjected to daily ML treatment (0.15 or 0.3 N, 1 Hz, 80% duty cycle, 10 min/day) beginning 1 day after injury (Fig. 2, A and D). Control animals were injured but not treated with ML. The load magnitude used in these studies was chosen on the basis of a previous study that evaluated the response of young TA muscle to a range of forces (0.15 to 0.6 N) that produced compressive strains of about 10 to 40% (*24*). To select the age range for the aged experimental group and to evaluate the response of muscle to loading as a function of age, we first assessed the bulk compressive mechanical properties of uninjured tissue from young (2- to 3-month-old), middle-aged (9- to 10-month-old), old (18- to 20-month-old), and very old (24- to 28-month-old) animals. Because the TA muscle did not exhibit significantly different bulk compressive mechanical properties with age (fig. S2), the age of animals used for further experimentation was selected on the basis of our target clinical population. Specifically, we used 20- to 22-month-old mice, which are roughly equivalent to 60- to 75-year-old humans, who would greatly benefit from robot-assisted mechanotherapies (*35*). This selection was further chosen on the basis of limited availability of animals more than 22 months old. Additional loading parameters (frequency, duty cycle, and load profile) for the current study were selected from the previously used range of ML parameters (*24*). In young animals, ML treatment resulted in significantly higher tetanic contraction forces and contraction velocities than in untreated controls after 14 days of treatment (Fig. 2, E to G). However, these beneficial effects on muscle function were not preserved with age. No significant differences in muscle function were observed in aged animals between ML-treated and untreated groups after 21 days of treatment, with elicited contraction forces and velocities remaining significantly lower than in injured young muscles (Fig. 2, F and G). Injured aged muscles treated with ML only reached about 20% of uninjured aged muscle forces and velocities throughout the duration of the study (21 days total).

Histological analysis revealed that ML significantly reduced the percentage of damaged myofibers and the degree of tissue fibrosis in injured young muscle. However, injured aged muscles still exhibited significant muscle damage and calcification with no improvement

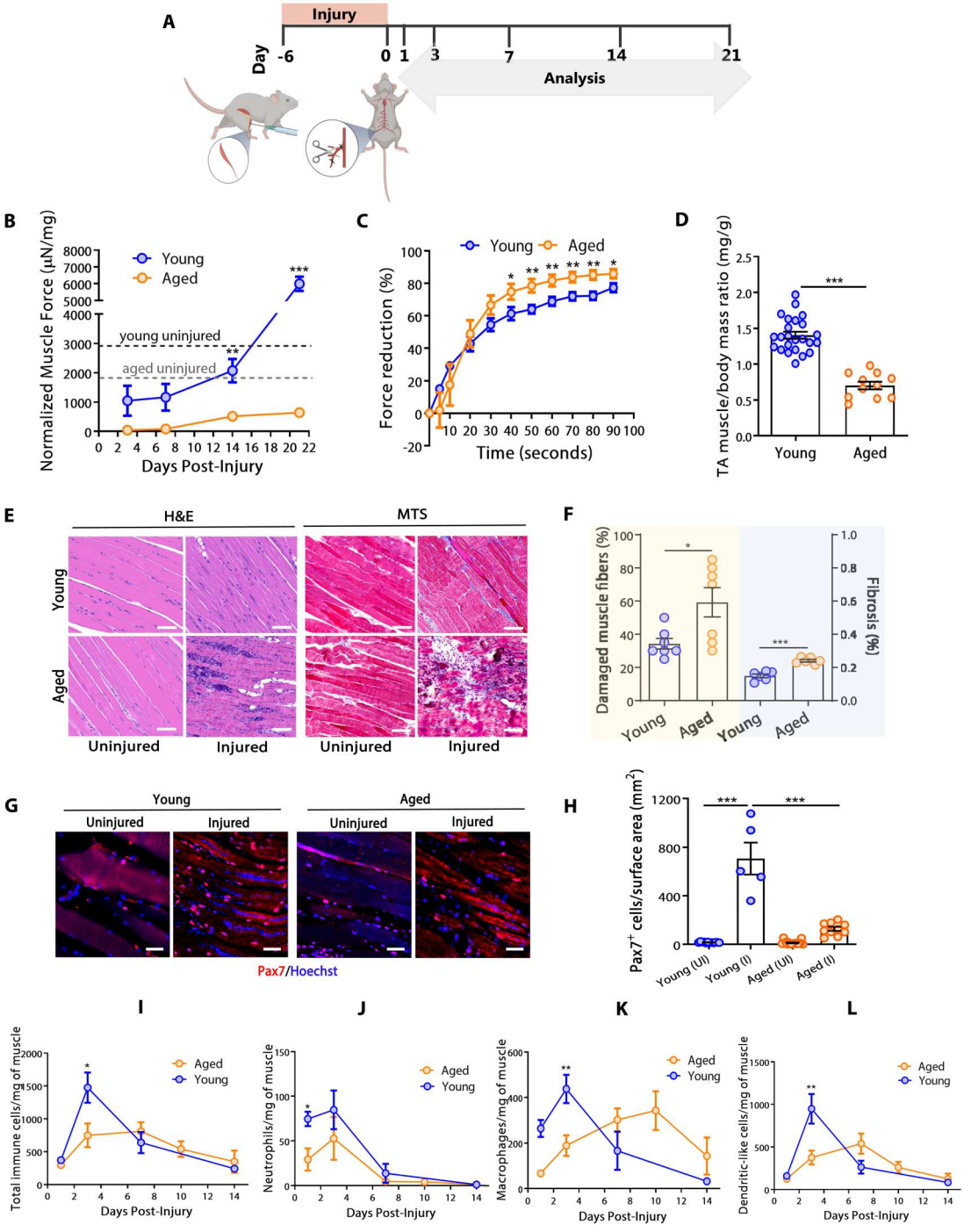

Fig. 1. Aged skeletal muscle exhibits impaired healing and poor inflammatory resolution after injury. (**A**) Experimental design and timeline of TA muscle injury and analysis. (**B**) Normalized tetanic contraction forces evoked from young and aged TA muscles across 21 days after injury. Dark gray and light gray dashed lines indicate the level of tetanic contraction forces from uninjured young and aged TA muscles, respectively. (**C**) Muscle fatigue profile determined as a reduction in tetanic contraction force over consecutive stimulations at 14 days after injury. (**D**) TA muscle–to–body mass ratio. (**E**) Representative H&E and Masson's trichrome (MTS) images of uninjured and injured young and aged TA muscles and (**F**) quantification of percentage of damaged muscle fibers and percentage of fibrosis at 14 days after injury. (**G**) Representative images and (**H**) quantification of $Pax7^+$ cells in uninjured (UI) and injured (I) young and aged TA muscles at 3 days after injury. Quantification of (**I**) total immune cells ($CD45^+$), (**J**) neutrophils ($CD11b^+/CD11c^-/F4/80^-/Ly6g^+/Ly6c^{int}$), (**K**) macrophages ($CD11b^+/CD11c^-/F4/80^+$), and (**L**) dendritic-like cells ($CD11b^+/CD11c^+$) across 14 days after injury in aged versus young TA muscle. $n = 6$ to 15 independent samples for muscle function testing and immune cell analysis, with Student's t test performed at each time point, $n = 10$ to 23 biologically independent samples per condition for muscle weight, and $n = 5$ to 11 biologically independent samples per condition for H&E, MTS, and Pax7 quantification, with one-way ANOVA performed with Tukey post hoc analysis; mean ± SE; $^*P < 0.05$, $^{**}P < 0.01$, and $^{***}P < 0.001$. Raw data for young animals in (I) to (L) were obtained from our previous publication (*24*) and reanalyzed.

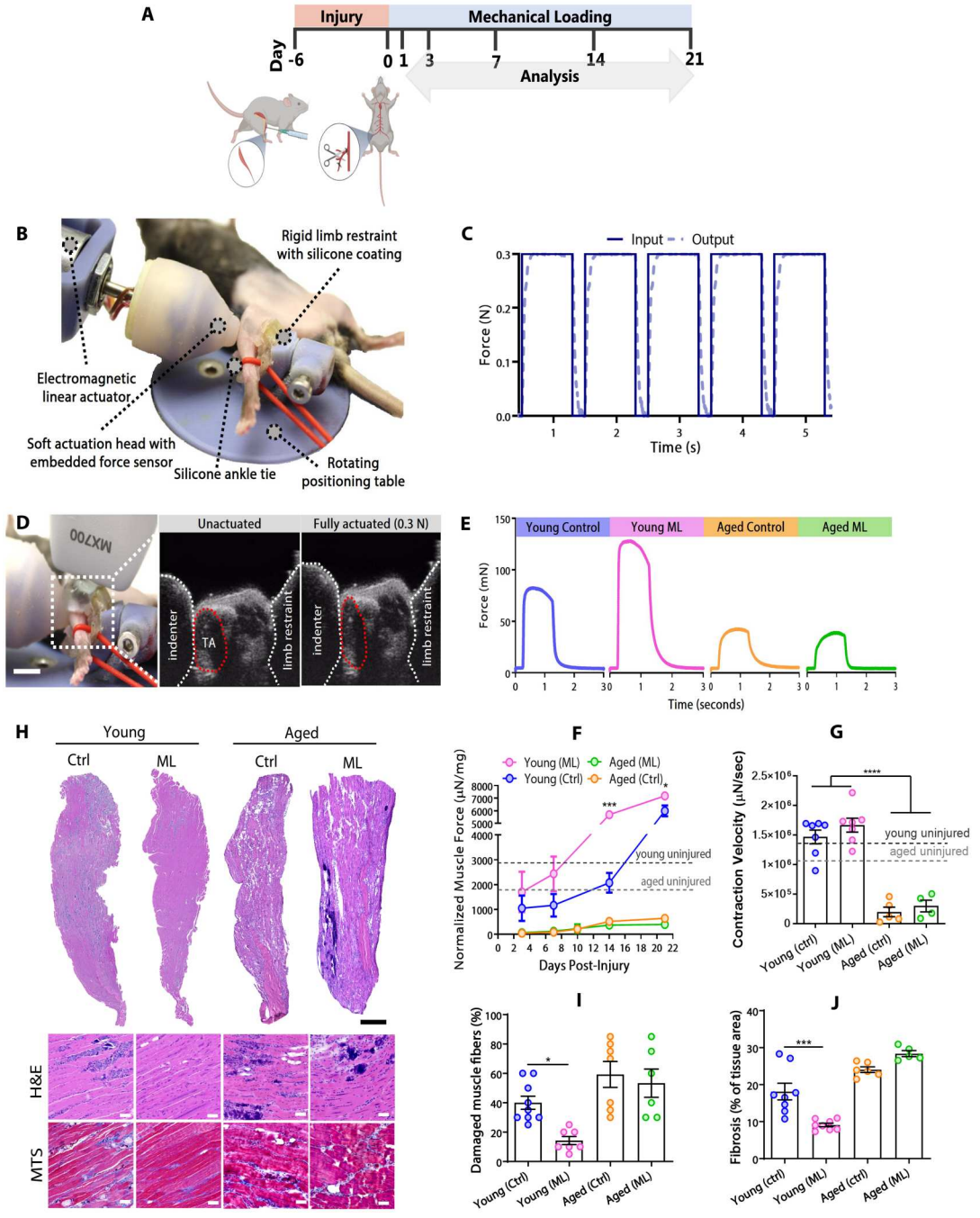

Fig. 2. Robot-actuated ML alone does not confer a positive therapeutic effect on aged muscle after injury. (**A**) Experimental design and timeline of TA muscle injury, ML treatment, and analysis. (**B**) Image of robotic ML device with a soft interface and integrated force sensor showing positioning of the actuator head over the TA muscle of the mouse hindlimb. The hindlimb was secured in a rigid U-shaped holster coated with a soft silicone interface, and the ankle was secured with a silicone tie to ensure repeatable positioning and to prevent limb deflection or translation. (**C**) Real-time force measurements at the actuator interface showing the commanded input force and actual output force (0.3 N). (**D**) Image of ultrasound integration capability during actuation of the device (left, scale bar: 1 cm), axial ultrasound image of mouse limb and unactuated indenter (middle), and axial ultrasound image of mouse limb and actuated indenter applying a load of 0.3 N to the TA muscle (right). (**E**) Representative force versus time profiles of tetanic muscle contractions from young and aged TA muscles in ML-treated versus control (Ctrl) groups at day 14 (control is injured but no ML). (**F**) Measurement of tetanic contraction forces across 21 days after injury and (**G**) contraction velocity at day 21. Dark gray and light gray dashed lines indicate the level of tetanic contraction forces from young uninjured and aged uninjured TA muscles, respectively. (**H**) Full-length longitudinal H&E sections and representative H&E and MTS images. Scale bars, 1 mm (full length) and 100 μm (regions). Quantification of (**I**) percentage of damaged myofibers and (**J**) percentage of fibrosis in control versus ML-treated young and aged TA muscle at 14 days after injury. $n = 4$ to 15 biologically independent samples per condition for muscle function testing, with Student's t test performed at each time point, and $n = 5$ to 9 biologically independent samples per condition for H&E and MTS quantification, with one-way ANOVA performed with Tukey post hoc analysis; mean ± SE; $^{*}P < 0.05$, $^{**}P < 0.01$, $^{***}P < 0.001$, and $^{****}P < 0.0001$. Raw data for young animals in (F) and (G) were obtained from our previous publication (*24*) and reanalyzed.

after ML (Fig. 2, H and I). The degree of fibrosis in injured aged muscles at 14 days after injury was significantly higher than in injured young muscles at the same time point, and a slight but not significant increase in fibrosis was observed in the ML-treated group in aged muscles compared with the untreated controls (Fig. 2, H and J). Despite a lack of functional response to ML in aged muscle, we still observed a notable up-regulation of YAP and MRTF-A mechanotransduction factors with loading (fig. S3). Hindlimb perfusion, as measured by laser Doppler imaging, was unchanged with ML in both young and aged animals; however, significantly slower perfusion recovery rates were observed in injured aged muscles, consistent with impaired revascularization processes with age (fig. S4). Further, the development of necrosis in the foot of the affected limb was minimal in young animals but

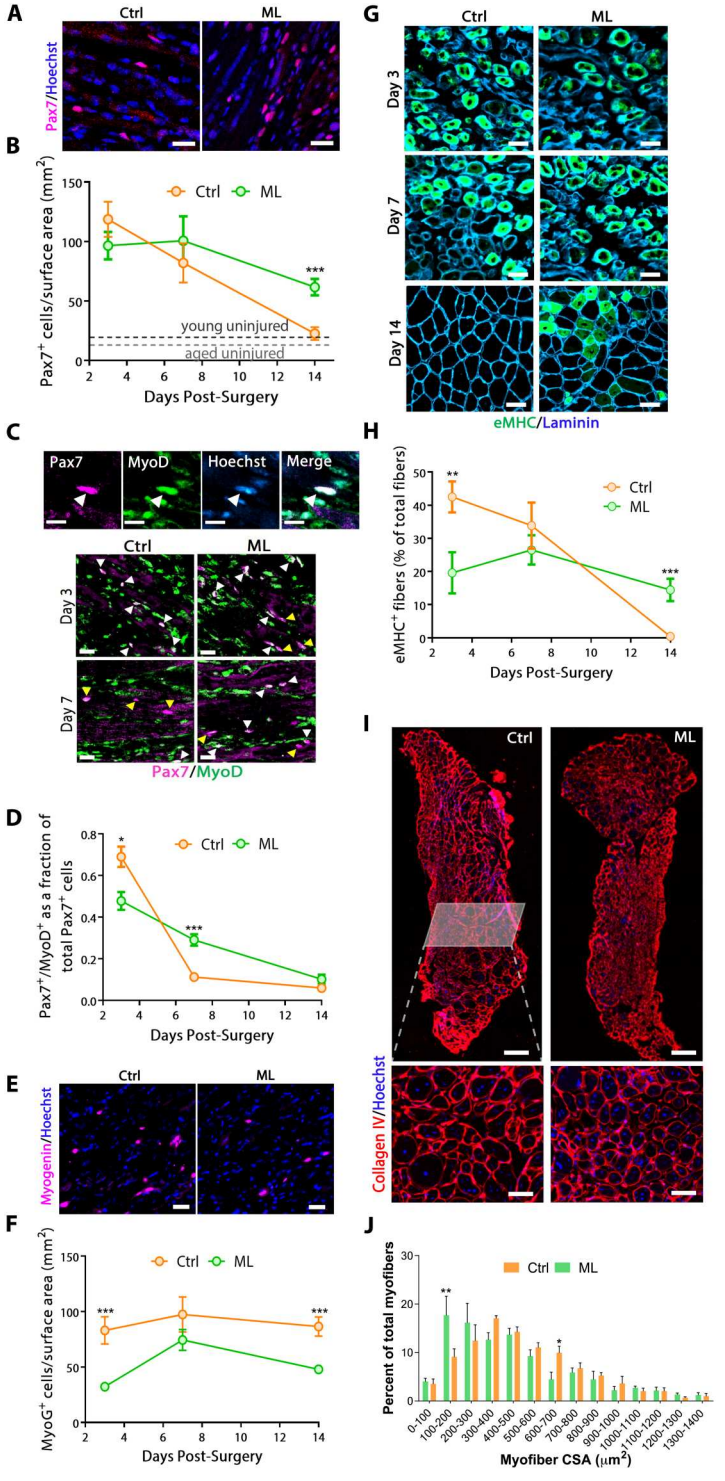

Fig. 3. ML disrupts the regenerative behavior of MPCs in aged skeletal muscle. (**A**) Representative images of Pax7$^+$ cells in control (Ctrl) versus ML (0.3 N) groups (scale bars, 20 μm) on day 14 and (**B**) quantification of Pax7$^+$ cells in injured aged muscle after 3, 7, and 14 days of ML treatment. (**C**) Representative images of Pax7$^+$/MyoD$^+$-stained cells showing cells labeled with (top, left to right) Pax7, MyoD, Hoechst, and a merge of all three nuclear stains (scale bars, 10 μm) and (bottom) control (Ctrl) versus ML-treated muscle (scale bars, 20 μm) on day 7 and (**D**) quantification of Pax7$^+$/MyoD$^+$ cells after 3, 7, and 14 days of ML. (**E**) Representative images of myogenin$^+$ (MyoG$^+$) cells in control versus ML-treated muscle (scale bars, 20 μm) on day 14 and (**F**) quantification of MyoG$^+$ cells after 3, 7, and 14 days of ML. (**G**) Representative images of eMHC$^+$ fibers after 3,7, and 14 days of ML (scale bars, 100 μm) and (**H**) quantification of eMHC$^+$ fibers across 3, 7, and 14 days of ML treatment. (**I**) Full-section images (top, scale bars, 300 μm) and representative regions (bottom, scale bars, 50 μm) of collagen IV–stained muscles and (**J**) histograms showing the distribution of myofiber CSA in control versus ML-treated tissues. Each bar in the histogram represents the percentage of total myofibers that fall into the indicated size bin. $n = 3$ to 5 biologically independent samples per condition, Student's t test performed at each time point; mean ± SE; $^*P < 0.05$, $^{**}P < 0.01$, and $^{***}P < 0.001$.

notable in aged animals and mildly worse in ML-treated aged muscles compared with controls (fig. S4). Muscle regeneration after this severe injury was also likely influenced to an extent by effects on peripheral nerves and neuromuscular synapses. Neural innervation after muscle injury is especially important to consider in the context of age, whereby reinnervation has been shown to be less efficient and effective (*36*–*38*). No significant age-dependent differences were observed in synapse density between young and aged muscle after 14 days of recovery (fig. S5). However, ML treatment led to an increase in the average synapse density of injured young muscle but not aged muscle, suggesting a potential mechanosensitivity of neuronal synapse formation in this injury model and the loss of this mechanism with age (fig. S5). To evaluate the possibility that the force magnitude of the ML treatment (0.3 N)

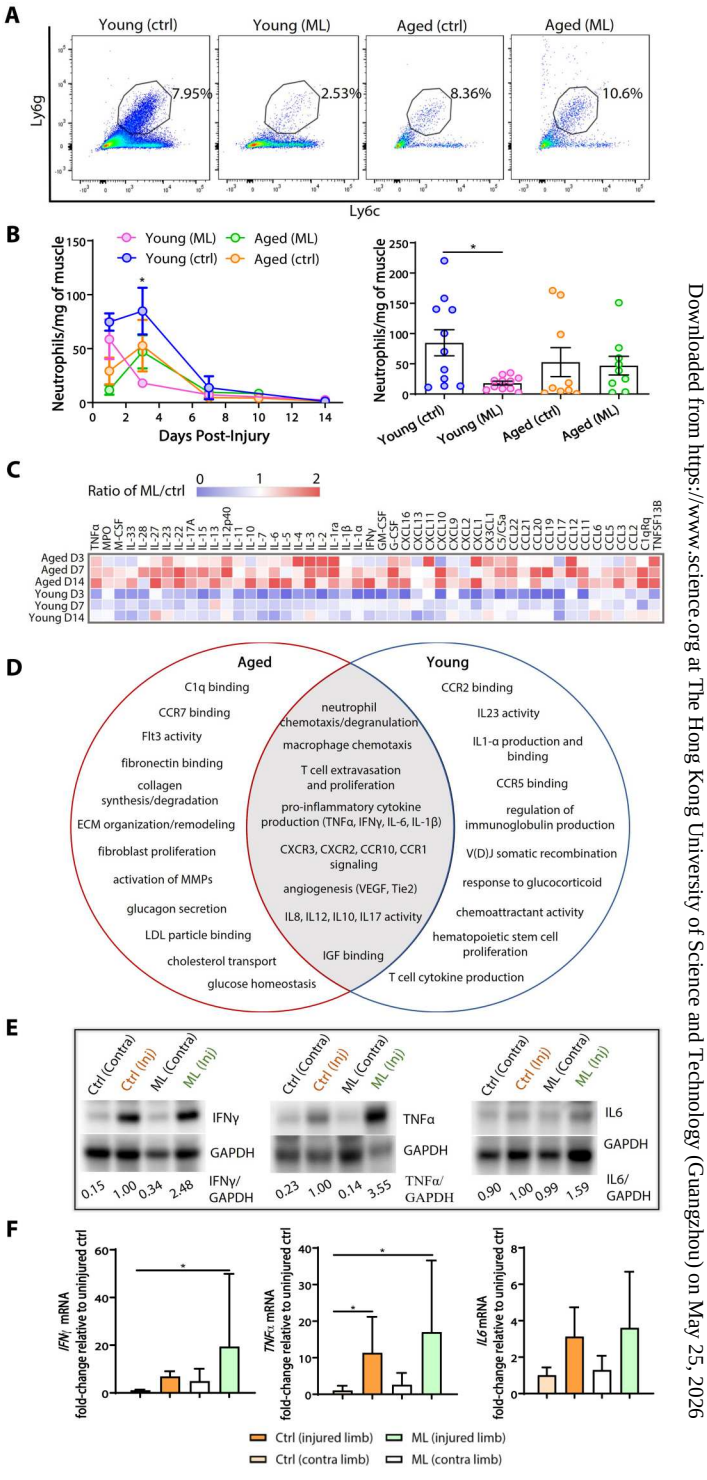

Fig. 4. The immune system is differentially regulated by ML in aged versus young muscle after injury. (**A**) Representative flow cytometry color dot plots of tissue neutrophils ($CD11b^+/CD11c^-/F4/80^-/Ly6G^+/Ly6C^{int}$) in control (Ctrl) versus ML-treated young and aged TA muscle on day 3. Inset values are the percentage of the gated population out of total $CD11b^+/CD11c^-/F4/80^-$ cells. (**B**) Quantification of tissue neutrophils across 14 days of treatment (left) and at day 3 (right) in young and aged TA muscle treated with or without ML. (**C**) Heatmap of expression levels of a subset of cytokines in injured young and aged TA muscle treated with or without ML for 3, 7, or 14 days (D3, D7, and D14). Values are a ratio of protein expression in ML-treated muscles normalized to protein expression in injured, untreated control muscles at the same time point. (**D**) Venn diagram highlighting biological processes and pathways identified through gene enrichment analysis of aged versus young muscle treated with ML compared with the control. Aged tissue–specific processes/pathways were enriched in proteins that exhibited a 1.5-fold increase in expression with ML compared with the control, and young tissue–specific processes/pathways were enriched in proteins that exhibited a 0.5-fold decrease in expression with ML compared with the control. The central portion of the Venn diagram represents processes/pathways that were enriched in proteins that exhibited 1.5-fold increase in aged tissue but a 0.5-fold decrease in young tissue with ML compared with the control. All processes/pathways shown had an FDR of $<1 \times 10^{-3}$ (PANTHER Gene Ontology Analysis). (**E**) Immunoblots of IFN-γ (left), TNFα (middle), and IL-6 (right) protein expression treated with or without ML along with the uninjured, untreated contralateral limb (Contra) obtained from the same set of animals. One biologically independent sample was run per condition, with all samples in a given experiment run on the same blot and stained in parallel. (**F**) qPCR data showing mRNA levels for IFN-γ (left), TNFα (middle), and IL-6 (right) in injured aged muscle treated with or without ML along with the respective uninjured, untreated contralateral limb. $n = 6$ to 15 biologically independent samples per condition for cell analysis, and $n = 3$ biologically independent samples per condition for qPCR. For cytokine analysis, tissue lysates were pooled from two biologically independent samples per condition, and one-way ANOVAs were performed with Tukey post hoc analysis; mean ± SE; $^*P < 0.05$, $^{**}P < 0.01$, $^{***}P < 0.001$. Raw data for young animals in (B) and (C) were obtained from our previous publication (*24*) and reanalyzed.

may be harmful for aged muscles, we tested the effects of lower compressive loads of 0.15 N on injured aged muscle using the same loading frequency, duty cycle, and load profile parameters. Consistent with 0.3-N loading, we did not observe any improvement in the functional recovery of injured aged muscle with the lower loading force (fig. S6). Together, these findings reveal important age-dependent effects of ML on muscle regeneration after severe injury.

ML disrupts the regenerative behavior of aged muscle stem cells during recovery

Because muscle stem cell activation, proliferation, and differentiation are essential for muscle regeneration to occur (*39*), we next evaluated aged stem cell behavior in response to ML after injury. The total number of cells expressing $Pax7^+$ across 14 days was highest in injured, untreated aged muscles (control) at 3 days

after injury and subsequently declined. However, ML-treated muscles exhibited a later peak in the $Pax7^+$ population at day 7, and by day 14, total $Pax7^+$ cells remained significantly higher in the ML-treated group, whereas the control group trended almost to baseline uninjured levels (Fig. 3, A and B). To determine the percentage of cycling $Pax7^+$ cells, we performed costaining with proliferation marker Ki67. At day 14, a significantly higher percentage of $Pax7^+$ cells in ML-treated aged muscles were also $Ki67^+$ compared with the controls, which no longer exhibited cycling $Pax7^+$ cells at that time point (fig. S7). These findings are consistent with data in Fig. 3 (A and B) that show that $Pax7^+$ cell numbers remained higher in ML-treated muscles compared with controls at day 14. Because most $Pax7^+$ cells observed after injury are MPCs beginning myogenesis, we quantified the fraction of $Pax7^+$ cells that also express MyoD, a myoblast determination protein that signals the myogenic commitment of an activated stem cell. $Pax7^+/MyoD^+$ double-positive cells also peaked early at 3 days after injury, indicating early expression of the MyoD transcription factor, and the fraction of cells expressing both markers subsequently declined in both ML-treated and control groups. However, a significantly higher fraction of $Pax7^+$ cells in the control group were $MyoD^+$ at day 3, followed by a more rapid decline leading to a significantly lower fraction of these double-positive cells in the control group by day 7 compared with the ML-treated group. By day 14, very few $Pax7^+$ cells expressed MyoD in either group (Fig. 3, C and D). Because it is known that the conversion of myoblasts into myocytes is accompanied by the expression of myogenin (MyoG), we quantified the number of MyoG-expressing cells. Throughout 14 days of treatment, higher numbers of $MyoG^+$ cells were observed in the control compared with the ML-treated group, with significant differences at days 3 and 14 (Fig. 3, E and F). By day 14, control muscles exhibited 3.8-fold lower numbers of $Pax7^+$ cells compared with $MyoG^+$ cells, whereas no difference was observed between these cell populations at the same time point in ML-treated muscles (fig. S8). These data suggest a delay in the conversion of $Pax7^+$ MPCs into terminally differentiating $MyoG^+$ myocytes in injured aged muscles treated with ML.

The maturity of muscle fibers was next analyzed. Once newly regenerated myofibers form, they begin to reexpress the embryonic isoform of myosin heavy chain (eMHC) (*40*). We observed that the percentage of $eMHC^+$ myofibers peaked in injured, untreated aged controls at day 3 compared with a later peak observed at day 7 in ML-treated aged muscles (Fig. 3, G and H, and fig. S9). By day 14, very few $eMHC^+$ myofibers were present in the controls, whereas ML-treated muscles still exhibited a significant number of actively regenerating $eMHC^+$ myofibers (0.4% versus 14.5% in control versus ML-treated groups, respectively) (Fig. 3, G and H, and fig. S9). We further analyzed myofiber cross-sectional area (CSA) in the aged muscles, which can provide a measure of muscle recovery because fiber size directly correlates with fiber maturity during healing (*41*). After 14 days of treatment, myofiber size histograms revealed a shift in the distribution of fiber size toward larger fiber CSA in control muscles. The controls exhibited a significantly higher percentage of larger (600 to 700 μm^2) mature fibers compared with ML-treated muscles, which exhibited a significantly higher percentage of small, immature muscle fibers (100 to 200 μm^2) (Fig. 3, I and J, and fig. S10). Figure S11 highlights the differences between ML-treated and control groups for each myofiber size bin. Furthermore, the percentage of centrally nucleated fibers, indicative of regenerated muscle fibers, was found to be lower in the ML-treated muscle compared with controls (fig. S12). These data indicate that injured, untreated aged control muscles are undergoing a more effective regeneration process compared with those treated with ML. Together, the evaluation of stem cell activation, proliferation, and differentiation in injured aged muscle suggests interference of ML treatment with normal cellular regenerative processes.

Inflammation is differentially regulated by ML in aged and young muscle after severe injury

To assess the effects of ML on the aged inflammatory response after severe muscle injury, we first quantified total immune cells and specific immune cell subpopulations within the damaged tissue using flow cytometry analysis (gating shown in fig. S13). In our previous work, treating injured young muscle with ML led to a significant reduction in tissue neutrophils at 3 days after injury, and we further linked this neutrophil clearance to the functional improvements observed in young animals (*24*). In contrast, here, we observed that injured aged muscle did not exhibit any changes in tissue neutrophil numbers or kinetics across 14 days of ML treatment (Fig. 4, A and B). In addition, there were no changes in cell number or kinetics for total aged immune cells ($CD45^+$), aged macrophages ($CD45^+/CD11b^+/F4/80^+$), or aged dendritic cells ($CD45^+/CD11b^+/CD11c^+$) (fig. S14). Macrophage subtypes (M1, M2a, and M2c) were similarly unaffected by ML treatment in injured aged muscle (fig. S15).

We next examined the expression of a broad range of cytokines and chemokines and determined their relative expression as a ratio of the ML-treated group to the untreated control (fig. S16 and table S1). We observed that, in injured young muscle, ML promoted down-regulation of numerous proinflammatory markers across 14 days of treatment. However, the opposite trend was observed in injured aged muscle, where ML produced an increase in most cytokines, with several exhibiting a trend of increasing expression from day 3 to day 14 (Fig. 4C). We confirmed that this effect is local to the ML-treated muscle by evaluating the expression of the same set of inflammatory markers in the sera of ML-treated animals (fig. S17 and table S2). Gene enrichment analysis of notably altered factors (either up-regulated or down-regulated by at least 50% with ML) in young versus aged muscle revealed that markers notably reduced in young muscle were largely involved in driving the inflammatory cascade through mechanisms such as CCR and CXCR binding or cytokine production, as well as mediating immune cell chemotaxis. In aged muscle, in contrast, many of the same markers were instead substantially increased with ML (Fig. 4D). We examined several proinflammatory markers more closely and observed increases in both mRNA and protein levels of interferon-γ (IFN-γ), tumor necrosis factor–α (TNFα), and interleukin-6 (IL-6) in injured aged muscles treated with ML compared with injured, untreated controls (Fig. 4, E and F). The expression of these three proinflammatory markers was also analyzed in the contralateral limb (uninjured, untreated limb) of the injured animal (control or ML-treated) to determine baseline levels of these cytokines and evaluate any potential systemic changes in response to ML applied to the injured limb (Fig. 4, E and F). Higher numbers of IL-6–expressing cells were also observed in muscles treated with ML for 7 days (fig. S18). Collectively, these data show that ML exerts age-dependent effects on the immune system through both a differential effect on immune

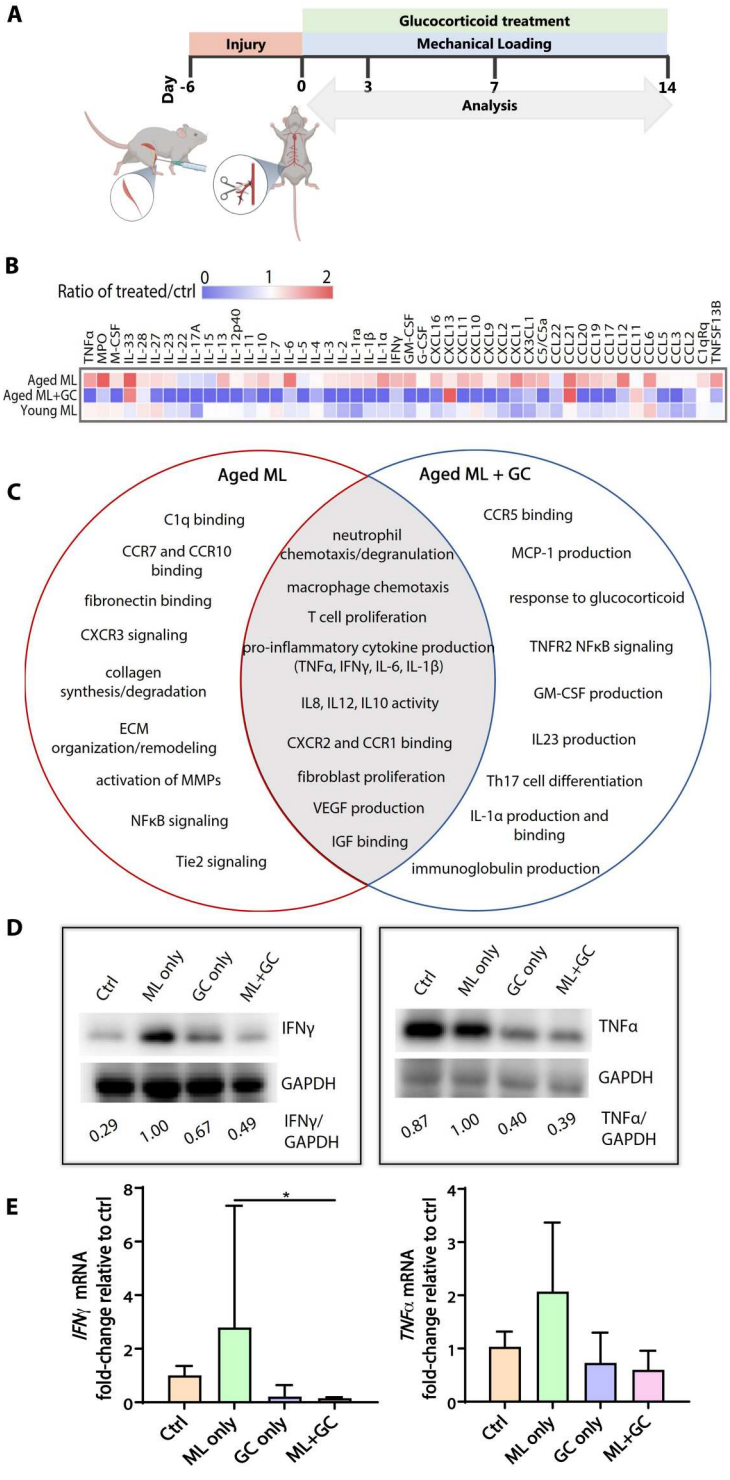

Fig. 5. GC treatment ameliorates ML-induced inflammation in aged muscle. (**A**) Experimental design and timeline of TA muscle injury, ML treatment with concurrent GC administration, and analysis. (**B**) Heatmap of expression levels of a subset of cytokines in injured aged TA muscle treated with ML only or ML + GC compared with injured young muscle treated with ML only. Values are expressed as a ratio of protein expression in the treated muscles normalized to protein expression in age-matched control muscles (injury only) at the same time point. (**C**) Venn diagram highlighting biological processes and pathways identified through gene enrichment analysis of aged muscle treated with ML compared with aged muscle treated with ML + GC. "ML-only" processes/pathways were enriched in proteins that exhibited a 1.5-fold increase in expression with ML compared with the untreated control, and "ML + GC" processes/pathways were enriched in proteins that exhibited a 0.5-fold decrease in expression with ML + GC compared with the untreated control. The central portion of the Venn diagram represents processes/pathways that were enriched in proteins that exhibited a 1.5-fold increase in ML-only–treated aged tissue but a 0.5-fold decrease in ML + GC–treated aged tissue compared with the untreated controls. All processes/pathways shown had an FDR of $<1 \times 10^{-3}$ (PANTHER Gene Ontology Analysis). (**D**) Immunoblots of IFN-γ (left) and TNFα (right) protein expression treated with ML only or ML + GC compared with GC only and untreated controls. One biologically independent sample was run per condition, with all samples in a given experiment run on the same blot and stained in parallel. (**E**) Quantitative PCR data showing mRNA levels for IFN-γ (left) and TNFα (right) in injured aged muscle treated with ML only or ML + GC compared with GC only and untreated controls. $n = 3$ or 4 biologically independent samples per condition for qPCR; for cytokine analysis, tissue lysates were pooled from two biologically independent samples per condition; one-way ANOVA with Tukey post hoc analysis, $^*P < 0.05$.

cell presence within the muscle and opposing effects on the proinflammatory cytokine cascade after injury—specifically, an ML-induced amplification of inflammation in aged muscle.

Results from the cytokine analysis also revealed other key differences between the responses of aged and young muscle to ML, specifically involving markers indicative of extracellular matrix remodeling and angiogenic processes. Different effects of ML were found on matrix metalloproteinases (MMPs), specifically MMP2, MMP3, and MMP9, in aged versus young regenerating muscle (fig. S19). A modest increase in the number of $MMP9^+$ cells in injured aged muscle was also found after 14 days of ML along with higher mRNA and protein expression levels, confirming results from the cytokine analysis. Furthermore, we observed significantly higher levels of fibronectin deposition in injured aged

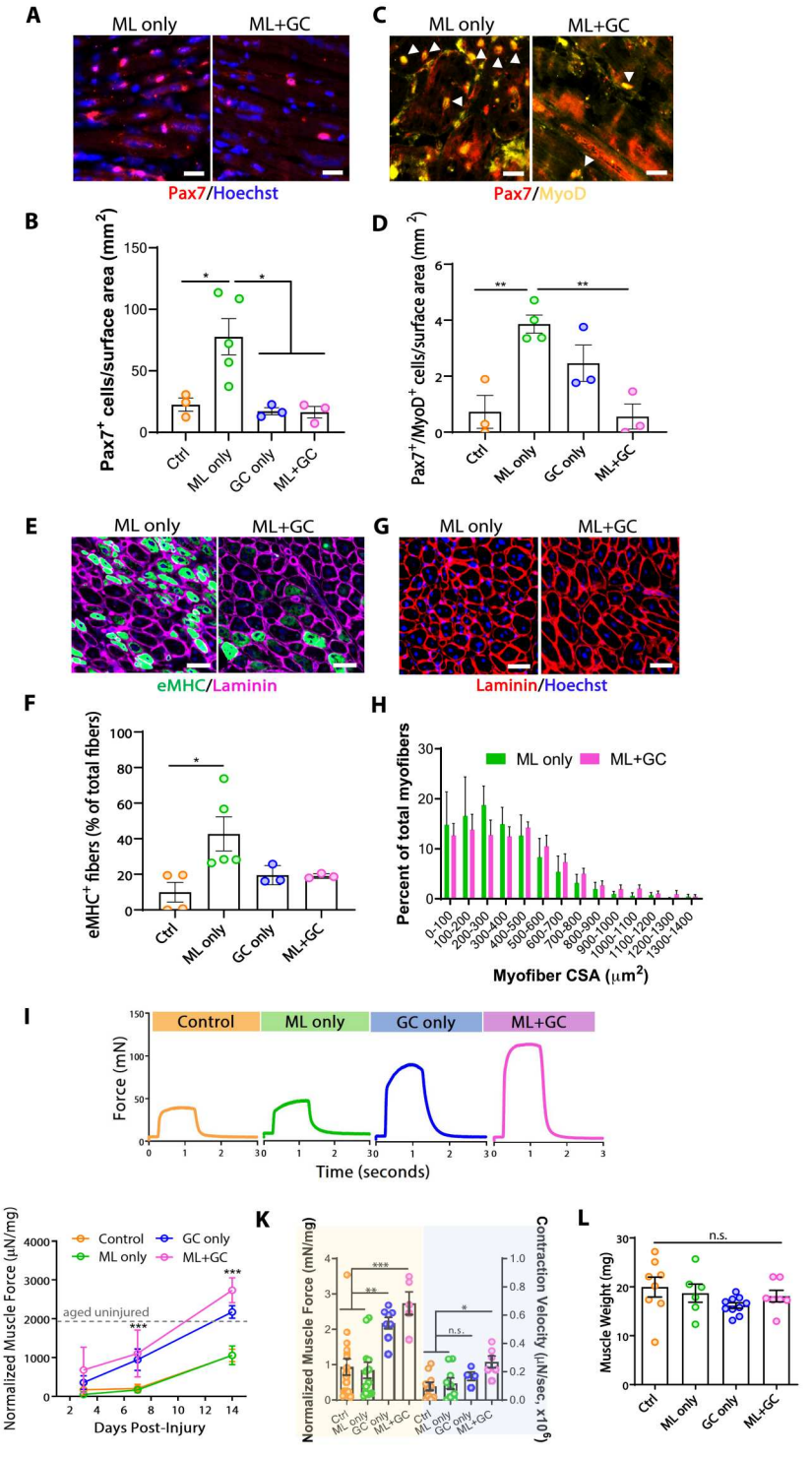

Fig. 6. Coupling ML with GC-mediated inflammatory control improves regenerative outcomes in aged muscle. Representative images and quantifications at day 14 of (**A** and **B**) Pax7$^+$ cells, (**C** and **D**) Pax7$^+$/MyoD$^+$ cells (indicated by white arrows), and (**E** and **F**) eMHC$^+$ myofibers in injured aged muscle treated with ML only versus ML + GC (scale bars: 20 μm for Pax7$^+$ and Pax7$^+$/MyoD$^+$, 50 μm for eMHC$^+$). (**G**) Representative regions (bottom, scale bars: 100 μm) of laminin-stained muscles and (**H**) histograms showing the distribution of myofiber CSA in aged muscle treated with ML only compared with ML + GC. Each bar in the histogram represents the percentage of total myofibers that fall into the indicated size bin. (**I**) Representative force versus time profiles of tetanic muscle contractions from injured aged muscles from control, ML-only, GC-only, and ML + GC groups (control is injured but no ML or GC). (**J**) Measurement of tetanic contraction forces across 14 days after injury. Light gray dashed lines indicate the level of tetanic contraction forces from uninjured aged TA muscles. Significance indicates ML + GC and GC-only groups compared with ML-only and untreated controls. (**K**) Maximum tetanic contraction force and velocity at day 14 and (**L**) muscle weight. $n = 3$ to 5 biologically independent samples per condition for Pax7, MyoD, and eMHC quantification, and $n = 5$ to 13 biologically independent samples per condition for muscle function analysis and muscle weight, one-way ANOVA performed with Tukey post hoc analysis; mean ± SE; $^*P < 0.05$, $^{**}P < 0.01$, $^{***}P < 0.001$, and $^{****}P < 0.0001$.

muscles treated with ML at 7 days after injury (fig. S19), as predicted by protein expression analysis. Angiogenesis was also regulated by ML in injured aged muscle, with significantly lower CD31$^+$ vessel density seen at later time points in ML-treated muscles compared with controls (fig. S20). Together, these findings reveal considerable age-dependent effects of ML on several important signaling pathways.

GC treatment coupled with ML improves regenerative outcomes in aged muscle

To test the hypothesis that ML-induced inflammation in aged muscle interferes with regeneration, we introduced anti-inflammatory therapy alongside ML treatment via systemic administration of the GC triamcinolone acetonide (TAc) (Fig. 5A). We first examined the same set of cytokines and chemokines after 14 days of treatment

(fig. S21 and table S3). Combining daily GC administration with ML alleviated the ML-induced inflammation in aged muscle by reducing the expression of several of these inflammatory markers in the injured tissue, many of which exhibited expression levels in ML + GC–treated aged muscle that were similar to those of young muscle treated with ML only (Fig. 5B and fig. S21). Gene enrichment analysis was performed on markers that were up-regulated by at least 50% in injured aged muscle treated with ML but then became down-regulated by at least 50% when ML was combined with GC treatment. This analysis revealed key pathways involved in immune cell chemotaxis, proinflammatory cytokine production, and chemokine activity, many of which were similarly down-regulated in injured young muscle treated with ML only (Fig. 5C). The effects of GC only on aged muscle inflammation during recovery were also evaluated and compared with ML-only and ML + GC treatments (fig. S22 and table S4). Enrichment analysis revealed several inflammatory processes shared by GC-only and ML + GC groups and a few that were unique to GC-only (fig. S23). Processes and pathways exclusive to the ML + GC group are also highlighted in fig. S23. Combining ML with GC treatment for injured aged muscle reduced the mRNA and protein expression levels of pro-inflammatory markers IFN-γ and TNFα, whose prolonged presence after injury has been shown to hinder muscle regeneration (Fig. 5, D and E) (*42*–*44*). To evaluate the mechanism driving this inflammatory suppression, we looked at the gene expression of nuclear factor κB (NF-κB), which is a transcriptional regulator of proinflammatory cytokine production and a known target of GCs (*45*, *46*), as well as the gene expression of a membrane-bound protein in the TNF receptor superfamily TNFRSF1b. As expected, the expression of both NF-κB and TNFRSF1b was elevated in the ML-only group compared with injured, untreated control muscles and significantly decreased in the ML + GC group compared with ML-only (fig. S24). Further evaluation of the cytokine profiling also revealed a notable reduction in markers involved in angiogenesis signaling, including vascular endothelial growth factor (VEGF) and Tie2, after 14 days of ML + GC treatment (table S3). The down-regulation of angiogenesis with ML + GC may be driven, in part, by self-regulating feedback, because ML + GC–treated animals exhibited significant improvements in hindlimb perfusion across 14 days compared with all other groups, as well as a notable reduction in hindlimb necrosis by day 7 (fig. S25). Together, these data demonstrate that GC therapy can reverse the negative effects of robot-actuated ML on aged muscle inflammation after injury, specifically preventing ML-induced up-regulation of several key proinflammatory markers through control of transcriptional regulation of cytokine production.

We next evaluated the behavior of aged muscle stem cells in response to the combined ML + GC treatment. Significantly lower levels of $Pax7^+$ MPCs were found in both GC-only and ML + GC groups compared with ML-only after 14 days (Fig. 6, A and B), as well as a significantly lower number of $Pax7^+/MyoD^+$ cells (Fig. 6, C and D). In addition, the percentage of myofibers that were $eMHC^+$ was reduced in GC-only and ML + GC groups compared with ML-only (Fig. 6, E and F). This reduction in actively differentiating myogenic precursors and lower numbers of immature $eMHC^+$ myofibers was observed concurrently with the appearance of larger, more mature myofibers in the ML + GC group as compared with ML-only, which is indicated by a rightward shift in the histogram of myofiber size distribution (Fig. 6, G and H). Figure S26 highlights the differences between ML-only and ML + GC groups for each myofiber size bin. GC-only treatment resulted in a more mature myofiber distribution compared with ML-only but not ML + GC, suggesting that the combination therapy is more effective than GC treatment alone at promoting aged muscle regeneration (fig. S27). The reduced inflammation, increased perfusion, reduced necrosis, and improved myogenic differentiation in aged muscle treated with ML + GC prompted us to evaluate whether ML in the presence of GC-mediated inflammatory control could improve aged muscle function after severe injury. After 7 days of treatment, we observed a significant improvement in the contractile force of injured aged muscles in both GC-only and ML + GC groups compared with both untreated controls and muscles treated with ML only (Fig. 6, I and J). By day 14, the ML + GC group exhibited higher average contractile force and velocity than all groups, including GC-only (Fig. 6, K and L). Furthermore, the effect of ML at the cellular level was still evident, because up-regulation of YAP and MRTF-A was found with ML regardless of the introduction of GC therapy (fig. S28). Together, these findings point to an inhibitory role of the aged inflammatory response in the regeneration of aged skeletal muscle after injury and the potential to alleviate the negative effects of robot-actuated ML on aged muscle regeneration using inflammatory control.

DISCUSSION

Age-dependent differences in the response of injured skeletal muscle to robot-actuated ML were found here, and a potential immunotherapeutic avenue to regenerate aged skeletal muscle with non-invasive mechanotherapy was identified. Although regenerative robotic strategies hold exciting promise for muscle repair, significant differences in how aged stem cells and aged immune cells respond to robot-actuated ML were revealed here that offer insight into how robotic-based mechanotherapies may best be translated with respect to increased patient age. Contrary to previous findings in young muscle, ML applied using a load-controlled robotic actuator produced no functional benefit in aged regenerating muscle and instead exacerbated tissue inflammation and perturbed aged muscle stem cell function. However, reducing inflammation using GC treatment mitigated the negative effects of ML on aged stem cells and enabled aged muscle response to this form of mechanotherapy, thus highlighting the importance of biological considerations, such as age, in the translation of robot-based technologies.

The regeneration of aged muscle after severe injury, in the absence of intervention, was found to be significantly impaired and associated with an altered inflammatory response. The reduced functional recovery and deficient aged muscle progenitor cell response to injury are consistent with numerous reports of age-imposed decline in muscle repair (*7*, *47*, *48*). The slow rate of immune cell infiltration into injured aged muscle, lower magnitude inflammatory response, and subsequent delayed immune cell egress are characteristic of inflammaging, whereby senescence leads to immune cell dysfunction and persistent low-grade inflammation (*10*, *11*, *49*).

In contrast to our previous studies in young animals (*24*), robot-mediated cyclic compressive loading did not promote functional recovery in aged skeletal muscle after injury. With respect to the inflammatory response, we revealed age sensitivity in the effects of ML on infiltrating immune cell populations. Unlike in young muscle,

ML did not lead to neutrophil clearance in aged tissue, nor did it affect the infiltration of other immune cell subtypes within injured aged tissue. Furthermore, a general inflammatory up-regulation was observed in aged muscle in response to ML treatment that contrasts the immunosuppressive effects of ML on young tissue (*20*, *21*, *24*, *25*, *50*). Numerous changes in immune cell phenotype have been documented with age that may contribute to the age-specific differences in response to ML, including phagocytic dysfunction and aberrant cytokine production—an overactivation of which may have contributed to the inflammatory up-regulation observed with ML. Furthermore, it is well known that muscle and its associated connective tissues stiffen with age, leading to alterations in force transmission (*51*–*53*), and this may make aged myofibers more susceptible to load-induced injury, potentially provoking a heightened release of myokines from the injured tissue in response to ML. The lack of functional improvement with ML in aged animals found here aligns with some studies in the literature that showed that aged muscle was unresponsive to massage-like therapy (*54*, *55*) but contradicts the findings of others (*18*, *56*, *57*). Because the methodologies used in past studies were highly inconsistent, these conflicting results may relate to the type of mechanical stimulus, loading regimen, injury model, and animal strain/age. These inconsistencies in part motivated our use here of a robotic system that allows precise and reproducible loading.

Age sensitivity of muscle stem cells to ML was also observed. In contrast to young muscle, where ML has been shown to promote myogenic activation and differentiation both in vivo and in vitro (*24*, *58*, *59*), aged muscle stem cell function was found to be disrupted by ML. Specifically, ML alone reduced the conversion of activated muscle stem cells into myoblasts and hindered differentiation and mature myofiber formation. Although age-associated intrinsic changes in muscle stem cell function, including cell cycle dysregulation and impaired signal transduction (*7*, *9*, *60*), may contribute to these age-specific effects, the disruption of myogenesis by ML in aged muscle is likely affected to a greater extent by the elevated inflammation observed after treatment. Inflammaging, which is associated with immune cell dysfunction that leads to a chronic persistent proinflammatory state, has been shown to disturb the local tissue environment and interfere with stem cell function and repair (*13*, *61*–*63*). In skeletal muscle, it has been demonstrated that muscle stem cells exhibit increased senescence and decreased function in response to elevated levels of proinflammatory cytokines (*64*). Factors such as TNFα, IFN-γ, IL-6, and IL-1 are consistently recognized as necessary for regeneration but detrimental when they persist at high levels (*42*–*44*, *65*, *66*).

As opposed to ML alone, combining ML with systemic GC therapy reduced the inflammatory profile in injured aged muscle, improved the differentiation of myoblasts and formation of more mature myofibers, and ultimately alleviated the negative effects of ML on aged muscle recovery. Although substantial literature exists on the efficacy of GCs for treating Duchenne muscular dystrophy (DMD) (*67*–*69*), this work uniquely demonstrates their restoring capacity in injured aged muscle. Our observations are consistent with findings of GC-mediated myogenesis in DMD via enhanced myoblast fusion and myotube formation (*70*). Other studies have found that treating aged muscle with high-dose sodium salicylate after injury partially reversed age-associated inflammation via inhibition of NF-κB, preventing the repression of myogenic differentiation and promoting aged muscle repair (*71*). Because GCs are known to also have a direct suppressive effect on NF-κB signaling (*46*), it is not surprising that this transcription factor is significantly altered by combining ML with GC, which likely contributes to alleviating the negative effects of ML alone on aged myogenesis. Along with a reduction in the TNF-receptor protein TNFRSF1b, this notion is further supported by a reduction in the expression of TNFα and IFN-γ after ML + GC treatment, which are two cytokines known to up-regulate NF-κB signaling (*72*).

Introducing GC therapy in combination with ML substantially improved aged muscle recovery after injury compared with ML only. Although the difference in muscle function between ML + GC and GC-only groups was not significant, greater significance was observed in contraction force for ML + GC versus ML-only groups compared with GC-only versus ML-only groups. Further, only the combination therapy resulted in significantly higher contraction velocity over the ML-only group. Throughout recovery, significant improvements in blood flow to the ischemic hindlimb with the ML + GC treatment were observed compared with all other groups. This observation is consistent with reports of GC-mediated enhanced endothelial function and vascularization (*73*), and these improvements likely contributed to the regenerative benefits in this severe injury model. These two observations of enhanced muscle function and greater vascular perfusion with ML + GC indicate that inflammatory control reverses the negative effects of ML on aged regenerating muscle and may permit aged muscle to respond to robot-actuated ML. We also observed appreciable increases in mechanotransduction factors YAP and MRTF-A in aged tissue after ML, which remained up-regulated with the combination ML + GC therapy.

In conclusion, this study revealed important age-dependent differences in the response of skeletal muscle to robot-actuated ML after severe injury and uncovered multiple negative effects of ML on aged muscle regeneration. The use of inflammatory control to guide aged muscle recovery in response to ML is a potentially powerful concept that is likely to be highly relevant to defining clinical studies for the elderly patient population. Although GC therapy can be accompanied by a range of potential adverse effects, the use of GCs in this work offers a proof of concept. Further investigation should focus on the use of a more targeted pharmacological aid in combination with ML, as well as a more in-depth assessment of the negative role of ML in aged muscle. Geriatric trauma is a field of medicine that stands to benefit substantially from robot-assisted tissue regeneration technologies. This work demonstrates the importance of using pharmaceutical control of age-associated biological changes as an adjunct to robot-based therapy to harness the value of regenerative robotics observed in young tissue for the aged.

MATERIALS AND METHODS

Robotic actuator design and fabrication

A robotic device used to apply cyclic compressive loading to the TA muscle of the mouse hindlimb was designed and fabricated as previously described (*24*). Briefly, the system used an electromagnetic linear actuator coupled with a force sensor to perform force feedback–controlled loading using a proportional-integral control (PID) algorithm implemented through a custom LabVIEW program (LabVIEW, National Instruments, USA). The force sensor (FS Series, Honeywell, USA) was embedded within a soft

actuation tip (Dragon Skin FX-Pro, SmoothOn, PA, USA) that interfaced with the surface of the TA muscle and provided a readout of the normal force at the tissue surface during each loading cycle. The mouse limb was restrained in a soft limb support and stabilized at the ankle using a silicone tie. The input signal from the force sensor was acquired via an input analog module (NI9205, National Instruments, USA) and processed through a signal amplifier (UV-10, Honeywell, USA). PID control was implemented via a real-time controller (cRIO-9030, National Instruments, USA) to create a digital controller output signal according to the desired input force. The analog signal was passed to the motor driver (950 series, MotiCont, CA, USA) via a digital-to-analog module (NI9264, National Instruments, USA). A host PC was used to input and adjust desired loading parameters, which included force magnitude, frequency, duty cycle, and load profile (square, sine, and triangular waveforms). Devices were calibrated before use using a precision scale (Ohaus Scout). Parameters used in this study were square wave with a frequency of 1 Hz, duty cycle of 80%, and variable force magnitude (0.15 or 0.3 N depending on the study). The actuator could be positioned to enable ultrasound imaging in real time during compressive loading. The TA muscle was imaged in the axial plane using a high-frequency ultrasound with a 50-MHz transducer (Vevo3100, VisualSonics) while the muscle was being compressed laterally to medially.

Experimental groups and study design

Female C57BL/6 mice from two different age groups were used in most of the experiments in this study. Young animals were 2 to 3 months old, and aged animals were 20 to 22 months old (Charles River Laboratories, National Institute on Aging). For mechanical testing on healthy muscle, two additional age groups were evaluated (9 to 10 and 24 to 28 months old). An injury was induced in the hindlimbs of both experimental and control groups, but only experimental groups received ML treatment, beginning 1 day after injury. Surgical procedures were performed by one individual to minimize variability, and animals were randomly assigned to groups. Sample sizes for each experiment are provided in the figure legends. All experimental conditions were kept constant, and control and experimental groups were treated equally and in parallel to eliminate bias. Endpoint selection was determined on the basis of prior testing performed using young animals (*24*). Animals were only excluded from the study if they met the Institutional Animal Care and Use Committee–determined criteria for required euthanasia, for example, limb auto-amputation, before the study endpoint. For all tests, tissue samples were collected immediately after euthanasia.

Skeletal muscle injury model

Skeletal muscle injury was induced in the right hindlimb of the animal using a multistep combination injury involving intramuscular injection of snake venom toxin (notexin from *Notechis scutatus scutatus*, Latoxan Laboratory, France) into the TA muscle followed 6 days later by hindlimb ischemia. This model has been well-established and used experimentally to generate severe injury characterized by myofiber necrosis prolonged by ischemia and is achieved in the absence of defects to the muscle stem cell pool (*26*). Before notexin injection, animals were anesthetized with intraperitoneal injection of ketamine (120 mg kg^{-1}) and xylazine (10 mg kg^{-1}), and toxin was injected at a concentration of 10 μg ml^{-1}. After 6 days, the TA muscle was scored on the basis of the degree of notexin injury severity and distributed randomly into experimental groups, and ischemia was induced in the right hindlimb by unilateral ligation of the external iliac and femoral artery and veins (without sparing the femoral nerve) using 5-0 Ethilon sutures as previously described (*24*, *29*). Animals were subsequently allowed to recover under a heat lamp until they became fully responsive. A laser Doppler perfusion imaging (LDPI) analyzer (PerisScan PIM II, Perimed AB, Sweden) was used before and immediately after surgery to measure blood perfusion of the ischemic limb relative to the contralateral to evaluate surgical efficacy. LDPI was subsequently performed every other day on both hindlimbs to monitor perfusion. Necrosis severity in the injured hindlimb was also assessed as indicated by progressive darkening of the toenails, toes, and forefoot, ultimately followed by auto-amputation in some animals. All animal procedures were performed in accordance with the Harvard University Faculty of Arts and Sciences Institutional Animal Care and Use Committee guidelines.

Robot-actuated ML

ML treatment was administered for 10 min each day to the TA muscles of the right hindlimbs (injured) of animals in the experimental groups. Loading parameters were either 0.3 or 0.15 N at 1-Hz frequency and 80% duty cycle with a square wave force profile. For each ML treatment, the animals were first anesthetized using isoflurane, and the injured limb was secured in the limb restrainer with the TA muscle oriented to face the actuator horizontally to allow full perpendicular contact of the actuator with the muscle surface. During ML of the experimental groups, the control group (injured, no ML) was exposed to isoflurane for the same total duration to ensure equivalent anesthetic exposure between groups. This process was repeated each day for a period of 1 to 21 days. Animals were returned to their cage to recover after the treatment.

Muscle function analysis

At each study endpoint, TA muscles were isolated and weighed, and muscle function was evaluated by testing the maximum tetanic contractile force of each tissue as previously described (*21*). Briefly, immediately after muscle isolation and weighing, one end of the sample was clamped by a microclip connected to a force transducer (FORT 25, WPI Inc., USA), and the other end was clamped by its distal tendon using a microclip mounted vertically between two steel rod electrodes (1.6-mm diameter, 21 mm long). To achieve physiologically relevant tension and length, we adjusted the muscle length using a micrometer. During testing, the muscle was bathed in a solution of physiologic saline maintained at a temperature of 37°C and continuously supplied with oxygen to preserve tissue viability. A custom LabVIEW program was used to deliver electrical stimulation and acquire data. A pulse wave (pulse width of 2 ms and train duration of 1 s) with specified voltage and frequency was delivered to the electrodes from a power amplifier (OSC USA 1310). Tetanic contraction was evoked with voltages of 30, 35, and 40 V with frequencies of 10 Hz/V. Between each stimulation, muscles were allowed to rest for 5 min. The maximum tetanic force of contraction was defined as the difference between the maximum force reading and the prestimulation baseline. In the setting of muscle injury, normalizing contraction force to either muscle mass or CSA can be problematic, because neither accounts for potential hypoxic cores in the tissue that may not contribute to force output (*74*) nor the presence of noncontractile connective

tissue, such as fibrosis, often found in regenerating muscle. Here, each maximum contraction force value was normalized to muscle mass, as is standard practice for ex vivo muscle function testing (*75*–*77*). Contraction velocity was defined as the slope of the line from prestimulation ($t = 0$) to the time of peak maximum tetanic force ($t = t_{max}$).

Mechanical characterization of healthy skeletal muscle

The mechanical properties of healthy skeletal muscle were evaluated in the TA muscles of mice from four different age groups (2- to 3-month-old, 9- to 10-month-old, 18- to 20-month-old, and 24- to 28-month-old). Freshly isolated TA muscle was biopsy-punched to obtain a disk-shaped sample 3 mm in diameter. The thickness of each individual sample was measured before testing. The tissue was kept hydrated and immediately subjected to compression testing (Bose TA ElectroForce 3200; load cell: 250 g). Before we started the measurements, the muscle samples were surrounded with Dulbecco's Modified Eagle Medium to prevent drying and subsequently preloaded with a force of 1 g. An incremental stress relaxation and dynamic mechanical analysis was then completed at increments of 5% strain. Briefly, a ramp of 0.5 mm s^{-1} was applied to compress the muscle to 5% strain followed by a 5-min-long period of dwelling to evaluate relaxation percentage and rate. Next, 20 cycles of dynamic loading at 1 Hz (0.5% strain amplitude) were applied to evaluate the dynamic modulus and the tangent loss. This process was repeated at 10, 15, and 20% strain. During loading, the force, time, and displacement data were captured (WinTest v7) and subsequently analyzed using a custom MATLAB script for further processing.

Histology and immunofluorescence analysis

For histological analysis, isolated TA muscles were fixed with 4% paraformaldehyde (PFA), washed, paraffin-embedded, sectioned at a thickness of 10 to 12 μm, and stained with H&E or Masson's trichrome. For immunofluorescence staining, isolated TA muscles were snap-frozen in liquid nitrogen–cooled isopentane, embedded in optimal cutting temperature, and sectioned at a thickness of 10 to 12 μm to obtain cross sections at the mid-belly of the muscle as well as longitudinal sections. For staining, sections were rehydrated in phosphate-buffered saline (PBS) and subjected to antigen retrieval consisting of 10 min of boiling in citrate buffer (pH 6.0). The sections were then permeabilized with PBS–0.05% Triton-X and blocked in 3% bovine serum albumin with 5% normal goat serum, followed by mouse-on-mouse specific blocking (M.O.M. kit, Vector Laboratories). The sections were incubated overnight with primary antibodies, followed by washing and staining with fluorescently labeled immunoglobulin G (IgG) secondary antibodies and treated with a nuclear counterstain. The following reagents were used for immunofluorescence staining: anti-Pax7 (ab187339, Abcam), anti-laminin (ab11575, Abcam), anti-MyoD (ab16148, Abcam), anti-myogenin (ab124800, Abcam), anti-YAP1 (ab205270, Abcam), anti-MMP9 (ab228402, Abcam), anti-CD31 (ab124432, Abcam), anti-fibronectin (sc-271098, Santa Cruz Biotechnology), anti-eMHC [F1.652, Developmental Studies Hybridoma Bank (DHSB)], anti–IL-6 (ab208113, Abcam), anti-neurofilament (ab254348, Abcam), anti-synaptophysin (ab32127, Abcam), Alexa Fluor 647 goat anti-rabbit IgG (A32733, Invitrogen), Alexa Fluor 568 goat anti-mouse IgG (A11004, Invitrogen), Alexa Fluor 488 goat anti-mouse IgG (A32723, Invitrogen), and Hoechst 33342 (H3570, Thermo Fisher Scientific) as a nuclear counterstain.

Image analysis

For H&E and Masson's trichrome staining, entire tissue sections were imaged with a slide scanner (Zeiss Axioscan Z1) using a 20× objective in bright-field mode and automatically tiled in Zen Blue software. Evaluation of tissue damage, inflammatory infiltrate, and fibrosis from H&E and Masson's trichrome–stained tissues was performed in a blinded fashion by a pathologist at Harvard Medical School/Dana Farber. Sections were quantified for percentage of damaged fibers and fibrosis by color deconvolution followed by thresholding using ImageJ analysis software [National Institutes of Health (NIH)]. For immunofluorescence images, entire tissue sections were imaged similarly as described above using a slide scanner and 20× objective in fluorescence mode using the same image settings across samples. To quantify muscle fiber size, full cross-sectional images of TA muscle sections were divided into regions of interest (ROIs). ROIs were then processed using a Muscle Morphometry ImageJ plugin to quantify the number and size of myofibers in each tissue section. To quantify the number of $Pax7^+$, $MyoD^+$, $myogenin^+$, YAP^+, $IL\text{-}6^+$, and $MMP9^+$ cells, full longitudinal images were divided into ROIs that were thresholded in each channel to identify the protein of interest and the nuclear area and subsequently counted using ImageJ cell counter. Cell counts were then normalized by the total tissue area. For quantification of $eMHC^+$ fibers, ROIs for full muscle cross sections were analyzed using MyoVision software to count and measure myofibers expressing a minimum intensity of eMHC stain. All image quantification was performed on full-section images (either longitudinal or cross-sectional) by subdividing the entire tissue area into ROIs that were subsequently analyzed.

Immune cell population analysis

To evaluate the effects of ML on the presence and dynamics of intramuscular immune cell populations, flow cytometry analysis was performed. First, TA muscles were freshly isolated, minced, and digested using a skeletal muscle dissociation kit [magnetic-activated cell sorting (MACS), Miltenyi Biotec] and gentleMACS dissociator. Tissue lysate was then filtered through a 70-μm cell strainer to obtain a single-cell suspension, and cells were counted. The cells were then blocked with CD16/CD32 monoclonal antibody (eBioscience) and stained with the following primary antibodies: CD45–peridin chlorophyll protein (PerCP)/cyanine 5.5 (Cy5.5) (103132, BioLegend) or CD45–Pacific blue (103125 (BioLegend), CD11c–allophycocyanin (APC) (17-0114-81, Thermo Fisher Scientific), CD11b–phycoerythrin (PE)/Cy7 (25-0112-82, Thermo Fisher Scientific), F4/80-PE (12-4801-82, Thermo Fisher Scientific) or F4/80-PerCP/Cy5.5 (45-4802-82, Thermo Fisher Scientific), Ly6g–fluorescein isothiocyanate (FITC) (11-9668-82, Thermo Fisher Scientific), Ly6c–Pacific blue (128013, BioLegend), CD206-APC (141707, BioLegend), CD163-PE (12-1631-82, Thermo Fisher Scientific), and CD86-FITC (105005, BioLegend), all used at the manufacturer's recommended concentration. Cells were then washed and stained with LIVE/DEAD Fixable Near-IR stain (Thermo Fisher Scientific), fixed with 0.4% PFA, and stored at 4°C until they were run on a flow cytometer (LSR II, BD Biosciences). Controls used for gating included fluorescence minus one for each antibody, corresponding isotype controls, and unstained cells as a

negative control. Immune populations were defined as follows depending on the panel: macrophages ($CD45^+/CD11c^-/CD11b^+/F4/80^+$), monocytes ($CD45^+/CD11c^-/CD11b^+/F4/80^+/Ly6g^-$), dendritic-like cells ($CD45^+/CD11c^+/CD11b^+$), neutrophils ($CD45^+/CD11c^-/CD11b^+/F4/80^-/Ly6g^+/Ly6c^{int}$), M1 macrophages ($CD45^+/CD11b^+/F4/80^+/CD86^+$), M2a macrophages ($CD45^+/CD11b^+/F4/80^+/CD206^+$), and M2c macrophages ($CD45^+/CD11b^+/F4/80^+/CD163^+$), and gated as described in fig. S13.

Protein extraction and cytokine analysis

Tissue lysate was prepared from freshly isolated TA muscles by mincing and sonicating muscles in T-PER Tissue Protein Extraction Reagent (Thermo Fisher Scientific) containing a cocktail of protease and phosphatase inhibitors (Thermo Fisher Scientific). Tissue lysates were pooled from two samples per condition to obtain enough concentrated lysate for analysis. Protein concentration in the samples was determined using Pierce Bicinchoninic Acid Protein Assay Kit (23227, Thermo Fisher Scientific) according to the manufacturer's instructions. For cytokine screening, tissue lysate samples were collected from young and aged animals treated with ML for 3, 7, and 14 days. Serum samples were also collected by exsanguinating via cardiac puncture followed by sample clotting and centrifugation. Cytokine analysis was performed using the Proteome Profiler Mouse XL Cytokine Array (R&D Systems) to evaluate relative differences in the expression of 111 different mouse cytokines and chemokines between ML-treated and control samples. Controls were injured TA muscles that had not received ML. An equal amount of protein was loaded onto each cytokine membrane, and the arrays were processed according to the manufacturer's protocol. Densitometry analysis was performed using QuickSpots analysis software (Western Vision Inc.), and the relative expression for each protein was calculated as the ratio of expression in ML-treated samples to control samples for days 3, 7, and 14. Open-source matrix visualization software (Morpheus, Broad Institute) was used to plot a heatmap and perform hierarchical clustering. Gene enrichment analysis was conducted on proteins that were elevated by 50% or more in the ML-treated group compared with the control using the PANTHER Gene Ontology tool (http://pantherdb.org/) and cross-checked using ShinyGO v0.75 (http://bioinformatics.sdstate.edu/go/). Only enriched biological and molecular pathways with a false discovery rate (FDR) of 1×10^{-3} or less were considered.

Western blot

Tissue lysate was prepared from freshly isolated TA muscles by mincing and sonicating muscles in T-PER Tissue Protein Extraction Reagent (78510, Thermo Fisher Scientific) containing a cocktail of protease and phosphatase inhibitors (1861281, Thermo Fisher Scientific) supplemented with phenylmethylsulfonyl fluoride (0.1 mg/ml). Protein concentration in the samples was determined using Pierce Bicinchoninic Acid Protein Assay Kit (23227, Thermo Fisher Scientific) according to the manufacturer's instructions. Samples were prepared in Laemmli buffer (1610747, Bio-Rad) at a concentration of 2 μg/μl and boiled for 10 min before being loaded in a polyacrylamide gradient gel (4561086, Bio-Rad). After we separated proteins on the gel, they were transferred to nitrocellulose membrane at 100 V for 1 hour. The membrane was blocked with 5% nonfat milk in Tris-buffered saline with 0.1% Tween (TBS-T) for 1 hour and incubated with primary antibodies overnight at 4°C, followed by incubation at room temperature for 1 hour with horseradish peroxidase–conjugated secondary antibodies. Primary antibodies used for immunoblotting include IL-6 (ab208113, Abcam), IFN-γ (ab216642, Abcam), TNFα (ab1793, Abcam), MMP9 (ab38898, Abcam), YAP1 (ab205270, Abcam), MRTF-A (PA5-109960, Thermo Fisher Scientific), and glyceraldehyde-3-phosphate dehydrogenase (GAPDH) (ab9485, Abcam). Detection was performed using enhanced chemiluminescent detection reagent (34577, Thermo Fisher Scientific). Secondary antibodies used were goat anti-mouse IgG (405306, BioLegend) and donkey anti-rabbit IgG (406401, BioLegend). Densitometry analysis was performed using ImageJ to calculate the signal intensity of each band, which was normalized to GAPDH. In all immunoblots, one biologically independent sample was run per condition, with all samples for a given experiment run on the same blot and stained in parallel. Any cropping of blot images is specified in figure captions. No image adjustments were made, including alterations to brightness, contrast, or gamma output. Exposure time was kept constant within a given experiment for densitometry analysis. Uncropped scans of blots are provided in the Supplementary Materials.

RNA extraction and real-time reverse transcription qPCR

Total RNA was extracted from isolated TA muscles using the Aurum Total Fatty and Fibrous Tissues Kit following the manufacturer's protocol (7326830, Bio-Rad). RNA quality and concentration were assessed using spectroscopy (NanoDrop, Thermo Fisher Scientific). To prepare complementary DNA (cDNA), an iScript cDNA synthesis kit (Bio-Rad) was used with 1 μg of RNA per sample with the following thermocycler protocol: 25°C for 5 min,

Table 1. Primers used for reverse transcription qPCR.

Gene symbol	Gene ID (NCBI)	Forward primer	Reverse primer
IL6	16193	CTGCAAGAGACTTCCATCCAG	AGTGGTATAGACAGGTCTGTTGG
IFNγ	15978	AGACAATCAGGCCATCAGCAA	TGTGGGTTGTTGACCTCAAACT
MMP9	17395	GAGTCTTTGAGTCCGGCAGA	CTTCCAGTACCAACCGTCCTT
TNFα	21926	CAGAAAGCATGATCCGCGAC	CCATTTGGGAACTTCTCATCCC
p65NFκB	19697	AGGCTTCTGGGCCTTATGTG	TGCTTCTCTCGCCAGGAATAC
TNFRSF1bb	21938	GATGCCAAGGTGCCTCATGT	TCCGCCATGACTCTTGCTTG

46°C for 20 min, and 95°C for 1 min. For each quantitative polymerase chain reaction (qPCR) reaction, 2 μg of cDNA were used per sample with SYBR Green Chemistry (iTaq Universal SYBR Green Mastermix, Bio-Rad) in a CFX96 instrument (Bio-Rad) following the manufacturer's protocol: 95°C for 30 s, (95°C for 5 min and 60°C for 30 s) repeated for 40 cycles. Primers (listed in Table 1) were designed using Primer Blast (NIH), checked for sequence alignment using Nucleotide Blast (NIH), and synthesized by Sigma-Aldrich. To ensure amplification of a single product, a melt curve analysis was performed at the end of each run. Data were normalized by the Livak method using two reference genes, *Rps13* and *Tbp*. Gene expression levels were normalized to those of control samples at day 14 (*78*). Error was propagated with the formula $\text{Error}(a+b) = \sqrt{\text{Error}(a)^2 + \text{Error}(b)^2}$, and ΔCq values were used for statistical analysis.

In vivo GC delivery studies

To evaluate the effects of anti-inflammatory therapy in combination with ML on aged muscle regeneration, the GC TAc was administered to animals in conjunction with ML treatment. Starting on the day of surgery, animals were given TAc (1 mg/kg) via intraperitoneal injection and continued to receive TAc (1 mg/kg) daily for the duration of the study (total of 14 days). ML treatment was then administered for 10 min each day to the experimental groups as described above. Loading parameters were 0.3 N, 1-Hz frequency, and 80% duty cycle with a square wave force profile. Control groups (injury-only and ML-only) received an equal volume of 0.9% sterile saline via intraperitoneal injection daily. During ML of the experimental groups, the injury-only control and GC-only groups were exposed to isoflurane for the same total duration to ensure equivalent anesthetic exposure between groups.

Statistical analysis

Statistical analyses were performed using GraphPad Prism 9 (GraphPad Software). Student's *t* test was used to compare two groups. For comparing more than two groups, one-way and two-way analyses of variance (ANOVA) with post hoc Tukey's or Bonferroni's multiple comparisons were performed. The number (n) of biologically independent samples/animals is indicated in figure legends. For image analysis, blinding was performed whenever possible. No statistical methods were used to predetermine sample sizes, but sample sizes were similar to those reported in previous publications (*24*, *79*, *80*). All tests were two-sided, and statistical significance was determined using P values, with a value of <0.05 considered statistically significant ($^*P < 0.05$, $^{**}P < 0.01$, $^{***}P < 0.001$, and $^{****}P < 0.0001$).

Supplementary Materials

This PDF file includes:
Figs. S1 to S33
Tables S1 to S4
Reference (*24*)

Other Supplementary Material for this manuscript includes the following:
MDAR Reproducibility Checklist

REFERENCES AND NOTES

1. E. Volpi, R. Nazemi, S. Fujita, Muscle tissue changes with aging. *Curr. Opin. Clin. Nutr. Metab. Care* **7**, 405–410 (2004).
2. F. Hildebrand, H. C. Pape, K. Horst, H. Andruszkow, P. Kobbe, T. P. Simon, G. Marx, T. Schürholz, Impact of age on the clinical outcomes of major trauma. *Eur. J. Trauma Emerg. Surg.* **42**, 317–332 (2016).
3. A. H. Ringen, I. A. Gaski, H. Rustad, N. O. Skaga, C. Gaarder, P. A. Naess, Improvement in geriatric trauma outcomes in an evolving trauma system. *Trauma Surg. Acute Care Open* **4**, e000282 (2019).
4. L. Jiang, Z. Zheng, M. Zhang, The incidence of geriatric trauma is increasing and comparison of different scoring tools for the prediction of in-hospital mortality in geriatric trauma patients. *World J. Emerg. Surg.* **15**, 59 (2020).
5. G. P. Victorino, T. J. Chong, J. D. Pal, Trauma in the elderly patient. *Arch. Surg.* , 1093–1098 (2003).
6. B. D. Cosgrove, P. M. Gilbert, E. Porpiglia, F. Mourkioti, S. P. Lee, S. Y. Corbel, M. E. Llewellyn, S. L. Delp, H. M. Blau, Rejuvenation of the muscle stem cell population restores strength to injured aged muscles. *Nat. Med.* **20**, 255–264 (2014).
7. J. V. Chakkalakal, K. M. Jones, M. A. Basson, A. S. Brack, The aged niche disrupts muscle stem cell quiescence. *Nature* **490**, 355–360 (2012).
8. N. A. Dumont, Y. X. Wang, M. A. Rudnicki, Intrinsic and extrinsic mechanisms regulating satellite cell function. *Development* **142**, 1572–1581 (2015).
9. P. Sousa-Victor, L. García-Prat, P. Muñoz-Cánoves, Control of satellite cell function in muscle regeneration and its disruption in ageing. *Nat. Rev. Mol. Cell Biol.* **23**, 204–226 (2022).
10. J. Hazeldine, J. M. Lord, P. Hampson, Immunesenescence and inflammaging: A contributory factor in the poor outcome of the geriatric trauma patient. *Ageing Res. Rev.* **24**, 349–357 (2015).
11. C. Franceschi, P. Garagnani, G. Vitale, M. Capri, S. Salvioli, Inflammaging and 'garb-aging'. *Trends Endocrinol. Metab.* **28**, 199–212 (2017).
12. J. Peake, P. Della Gatta, D. Cameron-Smith, Aging and its effects on inflammation in skeletal muscle at rest and following exercise-induced muscle injury. *Am. J. Physiol. Regul. Integr. Comp. Physiol.* **298**, R1485–R1495 (2010).
13. L. A. Perandini, P. Chimin, D. da Silva Lutkemeyer, N. O. S. Câmara, Chronic inflammation in skeletal muscle impairs satellite cells function during regeneration: Can physical exercise restore the satellite cell niche? *FEBS J.* **285**, 1973–1984 (2018).
14. C. P. Montalto, V. Bhargava, G. S. Hong, Use of complementary and alternative medicine by older adults: An exploratory study. *Complement. Health Pract. Rev.* **11**, 27–46 (2006).
15. M. J. Siddiqui, C. S. Min, R. K. Verma, S. Q. Jamshed, Role of complementary and alternative medicine in geriatric care: A mini review. *Pharmacogn. Rev.* **8**, 81–87 (2014).
16. R. Tatsumi, S. M. Sheehan, H. Iwasaki, A. Hattori, R. E. Allen, Mechanical stretch induces activation of skeletal muscle satellite cells in vitro. *Exp. Cell Res.* **267**, 107–114 (2001).
17. Y. Wang, J. Song, X. Liu, J. Liu, Q. Zhang, X. Yan, X. Yuan, D. Ren, Multiple effects of mechanical stretch on myogenic progenitor cells. *Stem Cells Dev.* **29**, 336–352 (2020).
18. E. R. Hunt, A. L. Confides, S. M. Abshire, E. E. Dupont-Versteegden, T. A. Butterfield, Massage increases satellite cell number independent of the age-associated alterations in sarcolemma permeability. *Physiol. Rep.* **7**, e14200 (2019).
19. K. H. Vining, D. J. Mooney, Mechanical forces direct stem cell behaviour in development and regeneration. *Nat. Rev. Mol. Cell Biol.* **18**, 728–742 (2017).
20. J. D. Crane, D. I. Ogborn, C. Cupido, S. Melov, A. Hubbard, J. M. Bourgeois, M. A. Tarnopolsky, Massage therapy attenuates inflammatory signaling after exercise-induced muscle damage. *Sci. Transl. Med.* **4**, 119ra13 (2012).
21. C. A. Cezar, E. T. Roche, H. H. Vandenburgh, G. N. Duda, C. J. Walsh, D. J. Mooney, Biologic-free mechanically induced muscle regeneration. *Proc. Natl. Acad. Sci. U.S.A.* **113**, 1534–1539 (2016).
22. N. Zhao, B. Liu, S. W. Liu, W. Zhang, H. N. Li, G. Pang, X. F. Luo, J. G. Wang, The combination of electroacupuncture and massage therapy alleviates myofibroblast transdifferentiation and extracellular matrix production in blunt trauma-induced skeletal muscle fibrosis. *Evid. Based Complement. Alternat. Med.* **2021**, 5543468 (2021).
23. C. Haas, T. A. Butterfield, S. Abshire, Y. Zhao, X. Zhang, D. Jarjoura, T. M. Best, Massage timing affects postexercise muscle recovery and inflammation in a rabbit model. *Med. Sci. Sports Exerc.* **45**, 1105–1112 (2013).
24. B. R. Seo, C. J. Payne, S. L. McNamara, B. R. Freedman, B. J. Kwee, S. Nam, I. de Lázaro, M. Darnell, J. T. Alvarez, M. O. Dellacherie, H. H. Vandenburgh, C. J. Walsh, D. J. Mooney, Skeletal muscle regeneration with robotic actuation-mediated clearance of neutrophils. *Sci. Transl. Med.* **13**, eabe8868 (2021).
25. C. Waters-Banker, T. A. Butterfield, E. E. Dupont-Versteegden, Immunomodulatory effects of massage on nonperturbed skeletal muscle in rats. *J. Appl. Physiol.* **116**, 164–175 (2014).
26. J. G. Tidball, Regulation of muscle growth and regeneration by the immune system. *Nat. Rev. Immunol.* **17**, 165–178 (2017).

27. S. T. Sicherer, R. S. Venkatarama, J. M. Grasman, Recent trends in injury models to study skeletal muscle regeneration and repair. *Bioengineering* **7**, 76 (2020).
28. C. Borselli, H. Storrie, F. Benesch-Lee, D. Shvartsman, C. Cezar, J. W. Lichtman, H. H. Vandenburgh, D. J. Mooney, Functional muscle regeneration with combined delivery of angiogenesis and myogenesis factors. *Proc. Natl. Acad. Sci. U.S.A.* **107**, 3287–3292 (2010).
29. B. J. Kwee, B. R. Seo, A. J. Najibi, A. W. Li, T. Y. Shih, D. White, D. J. Mooney, Treating ischemia via recruitment of antigen-specific T cells. *Sci. Adv.* **5**, eaav6313 (2019).
30. O. Halevy, Y. Piestun, M. Z. Allouh, B. W. C. Rosser, Y. Rinkevich, R. Reshef, I. Rozenboim, M. Wleklinski-Lee, Z. Yablonka-Reuveni, Pattern of Pax7 expression during myogenesis in the posthatch chicken establishes a model for satellite cell differentiation and renewal. *Dev. Dyn.* **231**, 489–502 (2004).
31. E. Rigamonti, T. Touvier, E. Clementi, A. A. Manfredi, S. Brunelli, P. Rovere-Querini, Requirement of inducible nitric oxide synthase for skeletal muscle regeneration after acute damage. *J. Immunol.* **190**, 1767–1777 (2013).
32. D. Hardy, A. Besnard, M. Latil, G. Jouvion, D. Briand, C. Thépenier, Q. Pascal, A. Guguin, B. Gayraud-Morel, J. M. Cavaillon, S. Tajbakhsh, P. Rocheteau, F. Chrétien, Comparative study of injury models for studying muscle regeneration in mice. *PLOS ONE* **11**, e0147198 (2016).
33. P. J. Muire, L. H. Mangum, J. C. Wenke, Time course of immune response and immunomodulation during normal and delayed healing of musculoskeletal wounds. *Front. Immunol.* **11**, 1056 (2020).
34. J. M. Peake, O. Neubauer, P. A. D. Gatta, K. Nosaka, Muscle damage and inflammation during recovery from exercise. *J. Appl. Physiol.* **122**, 559–570 (2017).
35. K. Flurkey, J. M. Currer, D. E. Harrison, Mouse models in aging research. *Mouse Biomed. Res.* , 637–672 (2007).
36. U. Kovačič, J. Sketelj, F. F. Bajrović, Chapter 26 age-related differences in the reinnervation after peripheral nerve injury. *Int. Rev. Neurobiol.* **87**, 465–482 (2009).
37. S. Aare, S. Spendiff, M. Vuda, D. Elkrief, A. Perez, Q. Wu, D. Mayaki, S. N. A. Hussain, S. Hettwer, R. T. Hepple, Failed reinnervation in aging skeletal muscle. *Skelet. Muscle* **6**, 29 (2016).
38. R. T. Hepple, C. L. Rice, Innervation and neuromuscular control in ageing skeletal muscle. *J. Physiol.* **594**, 1965–1978 (2016).
39. C. Lepper, T. A. Partridge, C. M. Fan, An absolute requirement for Pax7-positive satellite cells in acute injury-induced skeletal muscle regeneration. *Development* **138**, 3639–3646 (2011).
40. F. A. Rahman, S. A. Angus, K. Stokes, P. Karpowicz, M. P. Krause, Impaired ECM remodeling and macrophage activity define necrosis and regeneration following damage in aged skeletal muscle. *Int. J. Mol. Sci.* **21**, 4575 (2020).
41. K. M. Wisdom, S. L. Delp, E. Kuhl, Use it or lose it: Multiscale skeletal muscle adaptation to mechanical stimuli. *Biomech. Model. Mechanobiol.* **14**, 195–215 (2015).
42. S.-E. Chen, B. Jin, Y.-P. Li, C. S-e, TNF-α regulates myogenesis and muscle regeneration by activating p38 MAPK. *Am. J. Physiol. Cell Physiol.* **292**, C1660–C1671 (2007).
43. P. Muñoz-Cánoves, C. Scheele, B. K. Pedersen, A. L. Serrano, Interleukin-6 myokine signaling in skeletal muscle: A double-edged sword? *FEBS J.* **280**, 4131–4148 (2013).
44. R. C. J. Langen, A. M. W. J. Schols, M. C. J. M. Kelders, E. F. M. Wouters, Y. M. W. Janssen-Heininger, Inflammatory cytokines inhibit myogenic differentiation through activation of nuclear factor-κampt;Beta;. *FASEB J.* **15**, 1169–1180 (2001).
45. T. Liu, L. Zhang, D. Joo, S.-C. Sun, NF-κB signaling in inflammation. *Signal Transduct. Target. Ther.* **2**, 17023 (2017).
46. N. Auphan, J. A. DiDonato, C. Rosette, A. Helmberg, M. Karin, Immunosuppression by glucocorticoids: Inhibition of NF-κB activity through induction of IκB synthesis. *Science* **270**, 286–290 (1995).
47. H. Henze, M. J. Jung, H. E. Ahrens, S. Steiner, J. von Maltzahn, Skeletal muscle aging – Stem cells in the spotlight. *Mech. Ageing Dev.* **189**, 111283 (2020).
48. I. M. Conboy, T. A. Rando, Aging, stem cells and tissue regeneration: Lessons from muscle. *Cell Cycle* **4**, 407–410 (2005).
49. M. Pinti, V. Appay, J. Campisi, D. Frasca, T. Fülöp, D. Sauce, A. Larbi, B. Weinberger, A. Cossarizza, Aging of the immune system: Focus on inflammation and vaccination. *Eur. J. Immunol.* **46**, 2286–2301 (2016).
50. C. Waters-Banker, E. E. Dupont-Versteegden, P. H. Kitzman, T. A. Butterfield, Investigating the mechanisms of massage efficacy: The role of mechanical immunomodulation. *J. Athl. Train.* **49**, 266–273 (2014).
51. G. Lacraz, A.-J. J. Rouleau, V. Couture, T. Söllrald, G. Drouin, N. Veillette, M. Grandbois, G. Grenier, Increased stiffness in aged skeletal muscle impairs muscle progenitor cell proliferative activity. *PLOS ONE* **10**, e0136217 (2015).
52. L. Marcucci, C. Reggiani, Increase of resting muscle stiffness, a less considered component of age-related skeletal muscle impairment. *Eur. J. Transl. Myol.* **30**, 223–233 (2020).
53. D. C. Hughes, M. A. Wallace, K. Baar, Effects of aging, exercise, and disease on force transfer in skeletal muscle. *Am. J. Physiol. Endocrinol. Metab.* **309**, E1–E10 (2015).
54. D. W. Van Pelt, A. L. Confides, S. M. Abshire, E. R. Hunt, E. E. Dupont-Versteegden, T. A. Butterfield, Age-related responses to a bout of mechanotherapy in skeletal muscle of rats. *J. Appl. Physiol.* **127**, 1782–1791 (2019).
55. M. M. Lawrence, D. W. Van Pelt, A. L. Confides, Z. R. Hettinger, E. R. Hunt, J. J. Reid, J. L. Laurin, F. F. Peelor, T. A. Butterfield, B. F. Miller, E. E. Dupont-Versteegden, Muscle from aged rats is resistant to mechanotherapy during atrophy and reloading. *GeroScience* **43**, 65–83 (2021).
56. T. A. Hornberger, R. D. Mateja, E. R. Chin, J. L. Andrews, K. A. Esser, Aging does not alter the mechanosensitivity of the p38, p70S6k, and JNK2 signaling pathways in skeletal muscle. *J. Appl. Physiol.* **98**, 1562–1566 (2005).
57. S. Joanisse, J. P. Nederveen, J. M. Baker, T. Snijders, C. Iacono, G. Parise, Exercise conditioning in old mice improves skeletal muscle regeneration. *FASEB J.* **30**, 3256–3268 (2016).
58. M. Sanchez, T. R. Preston, Biomechanical signals upregulate myogenic gene induction in the presence or absence of inflammation. *Am. J. Physiol. Cell Physiol.* **293**, 117–124 (1980).
59. K. Kurokawa, S. Abe, K. Sakiyama, T. Takeda, Y. Ide, K. Ishigami, Effects of stretching stimulation with different rates on the expression of MyHC mRNA in mouse cultured myoblasts. *Biomed. Res.* **28**, 25–31 (2007).
60. A. S. Brack, P. Muñoz-Cánoves, The ins and outs of muscle stem cell aging. *Skelet. Muscle* **6**, 1 (2016).
61. R. Büttner, A. Schulz, M. Reuter, A. K. Akula, T. Mindos, A. Carlstedt, L. B. Riecken, S. L. Baader, R. Bauer, H. Morrison, Inflammaging impairs peripheral nerve maintenance and regeneration. *Aging Cell* **17**, e12833 (2018).
62. E. K. Merritt, M. J. Stec, A. Thalacker-Mercer, S. T. Windham, J. M. Cross, D. P. Shelley, S. Craig Tuggle, D. J. Kosek, J. Kim, M. M. Bamman, Heightened muscle inflammation susceptibility may impair regenerative capacity in aging humans. *J. Appl. Physiol.* **115**, 937–948 (2013).
63. R. S. Blanc, J. G. Kallenbach, J. F. Bachman, A. Mitchell, N. D. Paris, J. V. Chakkalakal, Inhibition of inflammatory CCR2 signaling promotes aged muscle regeneration and strength recovery after injury. *Nat. Commun.* **11**, 4167 (2020).
64. A. M. Josephson, V. Bradaschia-Correa, S. Lee, K. Leclerc, K. S. Patel, E. M. Lopez, H. P. Litwa, S. S. Neibart, M. Kadiyala, M. Z. Wong, M. M. Mizrahi, N. L. Yim, A. J. Ramme, K. A. Egol, P. Leucht, Age-related inflammation triggers skeletal stem/progenitor cell dysfunction. *Proc. Natl. Acad. Sci. U.S.A.* **116**, 6995–7004 (2019).
65. Z. Chen, B. Li, R. Z. Zhan, L. Rao, N. Bursac, Exercise mimetics and JAK inhibition attenuate IFN-γ-induced wasting in engineered human skeletal muscle. *Sci. Adv.* **7**, eabd9502 (2021).
66. E. M. Pietras, C. Mirantes-Barbeito, S. Fong, D. Loeffler, L. V. Kovtonyuk, S. Zhang, R. Lakshminarasimhan, C. P. Chin, J. M. Techner, B. Will, C. Nerlov, U. Steidl, M. G. Manz, T. Schroeder, E. Passegué, Chronic interleukin-1 exposure drives haematopoietic stem cells towards precocious myeloid differentiation at the expense of self-renewal. *Nat. Cell Biol.* **18**, 607–618 (2016).
67. T. Zhang, X. Kong, Recent advances of glucocorticoids in the treatment of Duchenne muscular dystrophy (Review). *Exp. Ther. Med.* **21**, 447 (2021).
68. C. Angelini, The role of corticosteroids in muscular dystrophy: A critical appraisal. *Muscle Nerve* **36**, 424–435 (2007).
69. S. Kourakis, C. A. Timpani, D. G. Campelj, P. Hafner, N. Gueven, D. Fischer, E. Rybalka, Standard of care versus new-wave corticosteroids in the treatment of Duchenne muscular dystrophy: Can we do better? *Orphanet J. Rare Dis.* **16**, 117 (2021).
70. N. McRae, L. Forgan, B. McNeill, A. Addinsall, D. McCulloch, C. Van Der Poel, N. Stupka, Glucocorticoids improve myogenic differentiation in vitro by suppressing the synthesis of versican, a transitional matrix protein overexpressed in dystrophic skeletal muscles. *Int. J. Mol. Sci.* **18**, 2629 (2017).
71. J. Oh, I. Sinha, K. Y. Tan, B. Rosner, J. M. Dreyfuss, O. Gjata, P. Tran, S. E. Shoelson, A. J. Wagers, Age-associated NF-κB signaling in myofibers alters the satellite cell niche and re-strains muscle stem cell function. *Aging* **8**, 2871–2896 (2016).
72. D. C. Guttridge, M. W. Mayo, L. V. Madrid, C. Y. Wang, J. Baldwin, NF-κB-induced loss of *MyoD* messenger RNA: Possible role in muscle decay and cachexia. *Science* **289**, 2363–2365 (2000).
73. I. Hörster, K. Weigt-Usinger, C. Carmann, K. Chobanyan-Jürgens, C. Köhler, U. Schara, A. A. Kayacelebi, B. Beckmann, D. Tsikas, T. Lücke, The L-arginine/NO pathway and homoarginine are altered in Duchenne muscular dystrophy and improved by glucocorticoids. *Amino Acids* **47**, 1853–1863 (2018).
74. S. Pecha, J. Koivumäki, B. Geelhoed, R. Kempe, E. Berk, A. Engel, H. Reichenspurner, T. Eschenhagen, U. Ravens, A. Kaumann, T. Christ, Normalization of force to muscle cross-sectional area: A helpful attempt to reduce data scattering in contractility studies? *Acta Physiol.* **224**, e13202 (2018).
75. M. C. Hogan, S. Kohin, C. M. Stary, R. T. Hepple, Rapid force recovery in contracting skeletal muscle after brief ischemia is dependent on O_2 availability. *J. Appl. Physiol.* **87**, 2225–2229 (1999).

76. P.-L. Hsieh, V. Rybalko, A. B. Baker, L. J. Suggs, R. P. Farrar, Recruitment and therapeutic application of macrophages in skeletal muscles after hind limb ischemia. *J. Vasc. Surg.* **67**, 1908–1920.e1 (2018).
77. K. A. Huey, S. A. Smith, A. Sulaeman, E. C. Breen, Skeletal myofiber VEGF is necessary for myogenic and contractile adaptations to functional overload of the plantaris in adult mice. *J. Appl. Physiol.* **120**, 188–195 (2016).
78. K. J. Livak, T. D. Schmittgen, Analysis of relative gene expression data using real-time quantitative PCR and the 2−ΔΔCT method. *Methods* **25**, 402–408 (2001).
79. Y. Saito, T. S. Chikenji, T. Matsumura, M. Nakano, M. Fujimiya, Exercise enhances skeletal muscle regeneration by promoting senescence in fibro-adipogenic progenitors. *Nat. Commun.* **11**, 889 (2020).
80. A. Sahu, Z. J. Clemens, S. N. Shinde, S. Sivakumar, A. Pius, A. Bhatia, S. Picciolini, C. Carlomagno, A. Gualerzi, M. Bedoni, B. Van Houten, M. Lovalekar, N. F. Fitz, I. Lefterov, A. Barchowsky, R. Koldamova, F. Ambrosio, Regulation of aged skeletal muscle regeneration by circulating extracellular vesicles. *Nat. Aging* **1**, 1148–1161 (2021).

Acknowledgments: We acknowledge C. Hellriegel and D. Richardson for assistance at the Harvard Center for Biological Imaging (HCBI). We also thank R. Bronson of the Harvard Rodent Histopathology Core for evaluation of histology sections, and we acknowledge the Dana-Farber/Harvard Cancer Center in Boston, MA, for use of the Rodent Histopathology Core resources. We thank I. de Lázaro for assistance with qPCR and use of protocols and primers, S. Nam for assistance with Western blot technique, and Z. Niziolek and J. Nelson of the Harvard Bauer Core for technical assistance with flow cytometry. We also acknowledge the College of Health Sciences at the University of Kentucky for use of MyoVision analysis software as well as the use of Biorender.com for generating the schematics in the figures. **Funding:** This work was supported by National Institute of Dental and Craniofacial Research grant R01DE013349 (to D.J.M.), Materials and Research Science and Engineering Centers from NSF grant DMR-1420570 (to D.J.M.), AR3T Regenerative Rehabilitation Pilot grant (to D.J.M.), National Institute of Arthritis and Musculoskeletal and Skin Diseases grant F31AR075367 (to S.L.M.), NIH grant K99AG065495 (to B.R.F.), and National Institute of General Medical Sciences awards T32GM007753 and T32GM144273. **Author contributions:** S.L.M. and D.J.M. conceived the study and designed the experiments. S.L.M. carried out most of the experiments and data analyses. B.R.S. conducted young animal muscle function and young animal immune cell studies/analyses. B.R.F. performed mechanical characterization. J.T.A. built and maintained the robotic device. E.B.R. assisted with in vivo studies, immunofluorescence, and image analysis. C.T.O. developed the muscle function analysis software. H.H.V. and C.J.W. provided scientific and technical feedback on the work. S.L.M. and D.J.M. wrote the manuscript. All authors reviewed and commented on the manuscript. **Competing interests:** D.J.M. and C.J.W. are inventors on patent/patent application (U.S. patent application no. 15/776,853, publication no. U.S. 2020/0222582) held/submitted by Harvard University/Wyss Institute for the device used in this study. B.R.F. has been a paid consultant for Amend Surgical and has the following interests: Limax Biosciences, equity; Amend Surgical, licensed intellectual property. **Data and materials availability:** All relevant data that support the findings in this study are available in this article or in the Supplementary Materials. Code is available at https://doi.org/10.5281/zenodo.7683381.

Submitted 13 July 2022
Accepted 28 February 2023
Published 22 March 2023
10.1126/scirobotics.add9369

Science Robotics

Anti-inflammatory therapy enables robot-actuated regeneration of aged muscle

S. L. McNamara, B. R. Seo, B. R. Freedman, E. B. Roloson, J. T. Alvarez, C. T. O'Neill, H. H. Vandenburgh, C. J. Walsh, and D. J. Mooney

Sci. Robot. **8** (76), eadd9369. DOI: 10.1126/scirobotics.add9369

Science Robotics (ISSN 2470-9476) is published by the American Association for the Advancement of Science. 1200 New York Avenue NW, Washington, DC 20005. The title *Science Robotics* is a registered trademark of AAAS.